MinEx CRC Limited
26 Dick Perry Avenue, Kensington, WA, 6151
PO Box 1130, Bentley, WA, 6102, Australia
admin@minexcrc.com.au

ABN: 66 625 533 913

MinEx CRC provides financial support to the value of $1K to promote Honours and Masters by Coursework projects that are aligned with the mission of MinEx CRC and to encourage young researchers toward a career in mineral exploration research. Projects are not restricted to MinEx CRC Participants and Affiliates.

Please note that the content of this thesis has not been subjected to peer-review and subsequent corrections.

Australian Government
Department of Industry, Science and Resources
Cooperative Research Centres Program

DECIPHERING THE ORIGIN OF HIGH CARBON SHALES: THE AMUNGEE ORGANOFACIES CONUNDRUM, VELKERRI FORMATION, GREATER MCARTHUR BASIN

Thesis submitted in accordance with the requirements of the University of Adelaide for an Honours Degree in Geology

Lesley Ellen Edwards

February 2024

THE UNIVERSITY of ADELAIDE

DECIPHERING THE ORIGIN OF HIGH CARBON SHALES: THE AMUNGEE ORGANOFACIES CONUNDRUM, VELKERRI FORMATION, GREATER MCARTHUR BASIN

ABSTRACT

The Mesoproterozoic (1.4 Ga) Velkerri Formation of the McArthur Basin contains a number of intervals rich in organic matter (with TOC values locally >10w.t%). These have been used as supporting evidence for a transient middle Mesoproterozoic global oxygenation event.
New geochemical data collected from Urapunga-4 were compiled with previously published data to;

a) illuminate the origin of these organofacies and to particularly understand why the shale preserve such large fluctuations in TOC over short stratigraphic distances, and
b) address the competing hypotheses.

The relationship between TOC and $\delta^{13}C_{(org)}$, shows that the TOC peaks in the Amungee Member, all three high organic shales (A, B, and C shales), are interpreted to be caused by primary production. However, the A shale was also interpreted to possibly be due to sediment input outpacing the increased carbon production. The B shale was interpreted to be a result of a small organic bloom that was immediately followed by a increased sediment supply that was likely from a storm event.
In addition, organic geochemical data and detrital U-Pb zircon and novel laser Rb-Sr dating from newly accessible core samples in the Beetaloo Sub-basin, combined with detailed sedimentology were used, along with previously published data from Urapunga-4, to verify whether this new core (ELT002) intersects the Velkerri Formation.
The depositional age of the new core and the difference in sedimentology and geochemistry between Urapunga-4 well, indicate that this new core likely intersects the Kyalla Formation rather than the Velkerri Formation.

KEYWORDS

Greater McArthur Basin, Wilton Package, Roper Group, Velkerri Formation, Amungee Member, Kyalla Formation, Rb-Sr dating, U-Pb dating, Organic carbon isotopes, Total Organic Carbon

TABLE OF CONTENTS

Deciphering the Origin of High Carbon Shales: the Amungee organofacies conundrum, Velkerri Formation, Greater McArthur Basin i
Abstract i
Keywords i
List of Figures 4
1. Introduction 5
2. Geological Setting/Background 7
2.1. McArthur Basin 7
2.2. Wilton Package 8
2.3. Roper Group 11
2.4. Velkerri Formation 15
2.5. Drill Core Urapunga-4 16
2.6 Drill Core ELT002 16
3. Methods 17
3.1 Sedimentology 17
3.2 U–Pb dating. 18
3.3 Rb–Sr dating 19
3.4 Pyrolysis and Rock Eval 19
3.5 Elemental Analysis 20
4. Observations and Results 21
4.1 Sedimentology 21
4.1.1 Urapunga-4 21
4.1.2 ELT002 22
4.2 Geochronology 24
4.2.1 U–Pb in Zircon 24
4.2.1(a) ELT002-SST04 24
4.2.1(b) ELT002-SST08 25
ELT002 26
4.3 Organic Geochemistry 27
Total Organic Carbon (TOC) and C(org) 27
4.3.1 ELT002 28
4.3.2 Urapunga-4 30
5. Discussion 32
5.1 What is the depositional environment of rocks in ELT002 and Urapunga-4? 32

5.1.1 ELT002 32
5.1.2 Urapunga-4 35
5.2 What process led to organic enrichment in the Upper Roper Group of ELT002 and Urapunga-4? 37
5.2.1 ELT002 38
5.2.2 Urapunga-4 39
5.3 What is the age of the rocks in ELT002? And what is their provenance? 41
6. Conclusions 47
7. Acknowledgments 49
8. References 49

9. Appendix……..……...……. start 54

LIST OF FIGURES

Figure 1: Regional geological domain map of Northern Territory of Australia superimposed on the top-to-basement. 8
Figure 2: Wilton Package generalised stratigraphy across the greater McArthur Basin. 10
Figure 3: Generalised stratigraphy of the Roper 12
Figure 4: Generalised stratigraphy of the Roper Group with corresponding ages previously dated. 14
Figure 5: 207Pb/206Pb ages of the youngest populations and youngest single zircon grain. 24
Figure 6: Kernel density estimate plots for ELT002-SST04 and ELT002-SST08 25
Figure 7: Concordance plot for (a) ELT002-SST04. And (b) ELT002-SST08. 26
Figure 8: Calculated isochrons from(a) ELT002_119, and (b) ELT002_807 27
Figure 9: ELT002 (a) TOC vs Depth, and (b) δ13C(org) vs Depth 28
Figure 10: Urapunga-4 (a) TOC vs Depth, and (b) δ13C(org) vs Depth 30
Figure 11: Genralised stratigraphy log of ELT002 with TOC and δ13C(org) values. 32
Figure 12: Genralised stratigraphy log of Urapunga-4 with TOC and δ13C(org) values. 35
Figure 13: (a) ELT002 all data $\delta^{13}C_{(org)}$) vs TOC against depth (m) and (b) ELT002 only the deeper samples $\delta^{13}C_{(org)}$) vs TOC against depth (m). 39
Figure 14: Urapunga-4 $\delta^{13}C_{(org)}$) vs TOC against depth (m), highlighted A, B, and C Shale 41
Figure 15: Age Window of deposition for the ELT002 core. 44
Figure 16: Multidimensional scaling (MDS) plot. 47

1. INTRODUCTION

The greater McArthur Basin (Close, 2014) is a regionally extensive Proterozoic basin that overlies the North Australian Craton. It is an extensive sedimentary system that spans the northern reaches of Australia, stretching from the northern part of the Northern Territory to north-eastern Western Australia and the north-western Queensland (Collins et al., 2019; Mukherjee et al., 2019). The basin includes Palaeoproterozoic to Mesoproterozoic successions of the McArthur and Birrindudu basins, the Tomkinson Province, and potentially the Lawn Hill Platform and South Nicholson Basin to the southeast. These are all interpreted to be contemporaneous systems. Yet the full extent of the greater McArthur Basin's sedimentary system is still being revealed. The basin itself preserves approximately a billion years of Earth history, spanning from ca. 1.82 Ga to 0.85 Ga (Rawlings 1999; Ahmad & Munson 2013; Munson 2016; Munson et al. 2018; Yang et al. 2018). The successions of the McArthur Basin hold significance for both mineral and petroleum exploration (Close et al., 2017; Revie, 2017; Baruch et al., 2018; Revie & Normington, 2020).

A particular focus is the ca. 1.5–1.3 Ga Roper Group of the McArthur Basin, primarily in the Kyalla and Velkerri Formations (Jackson et al. 1986; Yang et al., 2018, 2019, 2020; Bodorkos et al., 2020). This study concentrates on the Velkerri Formation (ca. 1.3 – 1.4 Ga), characterised by its deep-water facies (Abbott & Sweet, 2000). Within the Velkerri Formation, three main organofacies exist, where total organic carbon (TOC) levels reach up to 10 wt. % (Cox et al., 2016; Revie & Normington, 2020). However, the exact reasons behind these high TOC organofacies within the Velkerri Formation remain unclear. It is uncertain whether they are driven by primary production, controlled by flooding surfaces, mineralogy, or a combination of these factors (Cox et al., 2022). By seeking a better understanding of the Velkerri Formation, this work aims to provide valuable insights into the Mesoproterozoic paleoenvironments conducive to preserving these resources.

To investigate the Velkerri Formation, the work concentrates on two main boreholes. The first, Urapunga-4, was drilled in 1987, and is located in the McArthur Basin proper (fig. 1). It is considered the type-section for the Velkerri Formation (Jackson et al., 1986; Rawlings, 1999; Abbott & Sweet, 2000). Despite its designation as the type-section, there are few published data to help in the comprehension of the extreme paleoenvironmental conditions, observed within the Velkerri Formation. The second aspect of this study targets a recently drilled hole, ELT002 (drilled by BHP), located in the southeastern Beetaloo sub-basin (fig 1), where well-site geologists interpreted that ELT002 intersected the Velkerri Formation. Here, we employ a series of geochemical paleoenvironmental proxies, such as δ13C(org) and total organic carbon (TOC), to construct a comprehensive geochemical profile through Urapunga-4. This geochemical profile will then be applied to interpret successions of ELT002, aiming to confirm its intersection with the Velkerri Formation. To ensure rigorous analysis of ELT002, a multi-proxy approach is adopted. To determine depositional environment of sediments, detailed sedimentological logging and facies analyses were conducted. Additionally, detrital zircon U–Pb dating is used to constrain maximum depositional ages and determine potential provenance, and sedimentary pathways. Finally, in-situ Rb–Sr dating of shales is used to constrain minimum depositional age of the sediment.

Despite its economic significance, the Velkerri Formation presents a puzzling aspect regarding the accumulation and preservation of organic matter. This study aims to comprehend the formation of these organic-rich rocks and assess their lateral extent across the basin. Such insights will facilitate future investigation into comprehending the depositional systems and factors influencing productivity within the greater McArthur Basin.

2. GEOLOGICAL SETTING/BACKGROUND

2.1. McArthur Basin

The informally named greater McArthur Basin (Close, 2014) is a regionally extensive depositional area, where Palaeoproterozoic to Mesoproterozoic rocks occur and overlie the North Australia Craton. The rocks of the McArthur Basin unconformably overlie the Neoarchean to Palaeoproterozoic Pine Creek Orogen in the northwest, and the Paleoproterozoic Arnhem and Murphy provinces in the northeast and southeast respectively. The basin sequences are themselves overlain by the Neoproterozoic to Devonian Georgina Basin, and the Mesozoic Carpentaria and Arafura basins (Walter et al., 1995; Ahmad et al., 2013).

The original extent of the basin is poorly constrained, as most of the current basin boundaries are the result of younger tectonic uplift that have consequently resulted in the erosion of basin sequences. Based on recent geological reconstructions, at ca. 1.3 Ga the North Australian craton is in the mid to low latitudes, plausibly juxtaposed against Laurentia (North America), Siberia, and North China craton (Collins et al., 2019; Mukherjee et al., 2019). Collins et al. (2019) suggest that the boarder marine environment formed a large gulf, referred to as the McArther-Yanliao gulf.

Rawlings (1999) and Close (2014) subdivided the sedimentary successions of the greater McArthur Basin into five basin-wide depositional “packages”. Each package was characterised by similarities in age, stratigraphic position, lithofacies, and basin-fill geometry. The five packages include, in ascending stratigraphic order, the Paleoproterozoic Redbank, Goyder, Glyde packages, and the Mesoproterozoic Favenc and Wilton Packages.

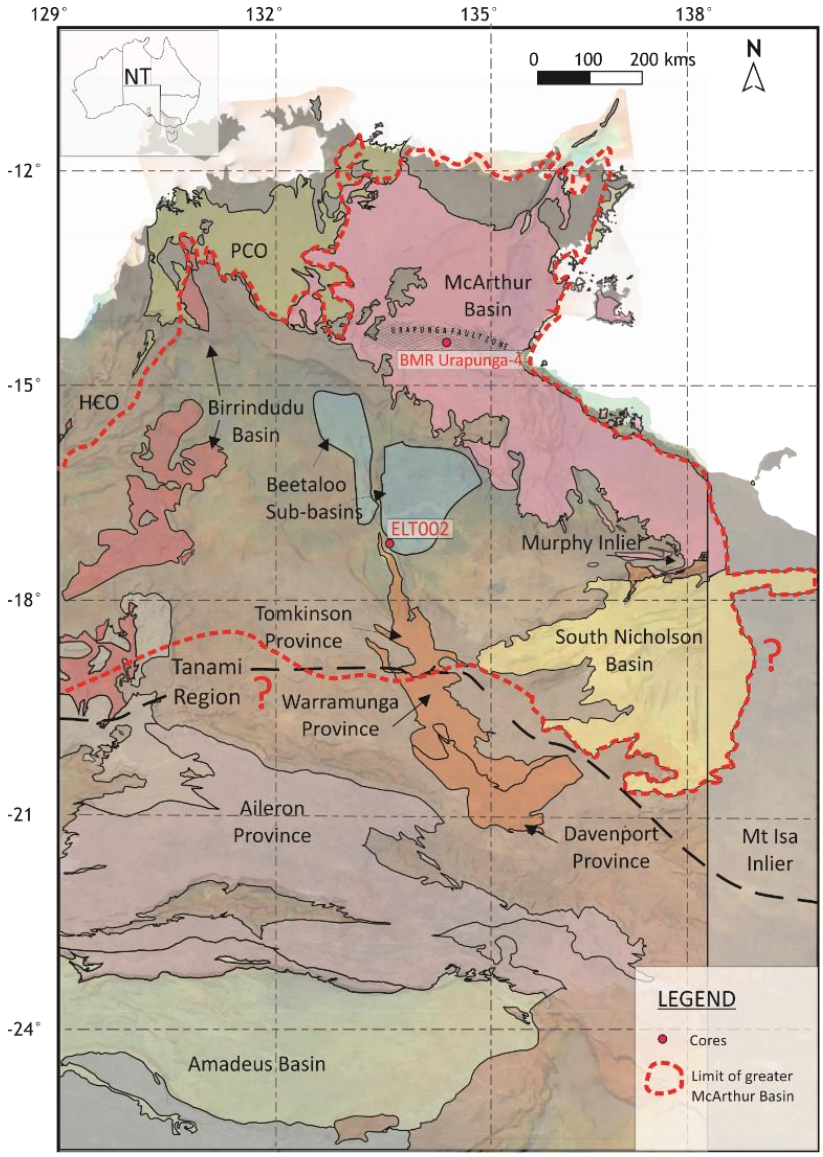

Figure 1: Regional geological domain map of Northern Territory of Australia superimposed on the top-to-basement (SEEBASE TIM basement surface image after Frogtech Geoscience, 2018) (Map modified from: Cox et al. 2022 & Blades M. pers comms)

2.2. Wilton Package

The middle Mesoproterozoic Wilton Package covers over 145,000 km^2 of the greater McArthur Basin (Abbott & Sweet, 2000). In seismic sections, the Wilton package is shown to be continuous in the subsurface and is interpreted to be preserved in several geographically separated basins (Williams, 2019). These continuous sedimentary successions of the Wilton

Package include the Roper Group of the McArthur Basin and Beetaloo Sub-basin, the Renner Group of the Tomkinson Province, the Tijunna Group of the Birrindudu Bain, and the South Nicholson Group in the South Nicholson Basin (Rawlings et al., 1999; Close, 2014; Munson, 2016; Munson et al., 2018).

The siliciclastic rocks of the Wilton Package are easily distinguishable from the underlying Favenc Package, where there are carbonate-dominated successions. The Wilton Package is dominated by alternating sandstone and mudstone units. The package has been interpreted to have been deposited in a range of depositional environments, which include, shoreline, shallow-marine to deep-marine shelf environments (Rawlings, 1999; Munson, 2016; Munson et al., 2018; Sheridan et al., 2018; Cox et al., 2022).

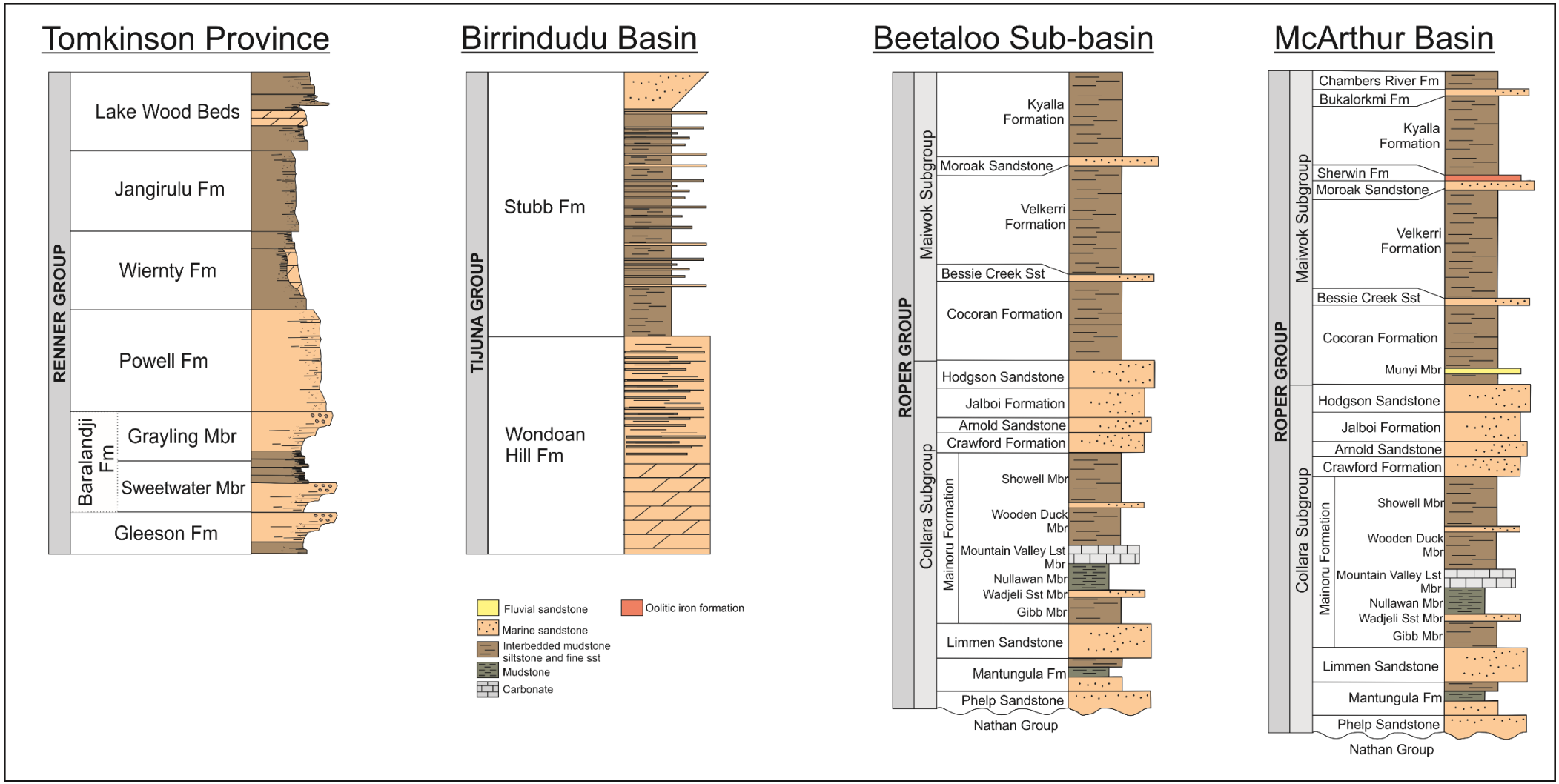

Figure 2: Wilton Package generalised stratigraphy across the greater McArthur Basin including, the Tomkinson Province, Birrindudu Basin, Beetaloo Sub-basin, and McArthur Basin.

2.3. Roper Group

The Roper Group, the McArthur equivalent of the Wilton package, is exposed in the McArthur Basin and in the subsurface of the Beetaloo Sub-basin (Ahmad & Munson, 2013; Munson, 2016; Williams, 2019).

It has significant lateral thickness changes across the McArthur Basin. The Roper Group is thinnest (<500m) over the north-south trending Batten Fault Zone and is ~1–2km thick near the Urapunga Fault Zone in the eastern Beetaloo Sub-basin (Plumb & Roberts, 1992; Abbott & Sweet, 2000; Rawlings et al., 2004; Munson, 2016; Williams, 2019), where it has been interpreted as the main depocenter of the Roper Group (Plumb & Wellman, 1987; Abbott & Sweet, 2000; Williams, 2019).

The Roper Group is subdivided into two subgroups, the Collara Subgroup, and the Maiwok Subgroup oldest to youngest, respectively (Rawlings, 1999; Abbott & Sweet, 2000). The subdivision was introduced to differentiate between tidal zone and platform sandstone-dominated and mudstone-dominated sequences. The Collara Subgroup, consisting of eight units, is dominated by sandstones, with minor mudstones, in ascending order: Phelp Sandstone, Mantungula Formation, Limmen Sandstone, Mainoru Formation, Arnold Sandstone, Jalboi Formation, and Hodgson Sandstone (Jackson et al., 1988; Rawling, 1999; Abbott & Sweet, 2000; Abbott et al., 2001; Munson, 2016). The Maiwok Subgroup is dominated by mudstones, less abundant in sandstones and consists of seven units. These include, in ascending order, Corcoran Formation, Bessie Creek Sandstone, Velkerri Formation, Moroak Sandstone, Kyalla Formation, the Bukalorkmi Sandstone, and the Chambers River Formation (Munson, 2016; Ahmad & Munson ,2013). The Roper Group has been interpreted to have been deposited in a low-energy shoreline-shelf environment, where the Maiwok Subgroup was deposited in slightly deeper shelf environments (Rawlings, 1999;

Abbott & Sweet, 2000). It has been envisaged as an enclosed marine basin with the modern analogue being the Black Sea (Cox et al., 2016).

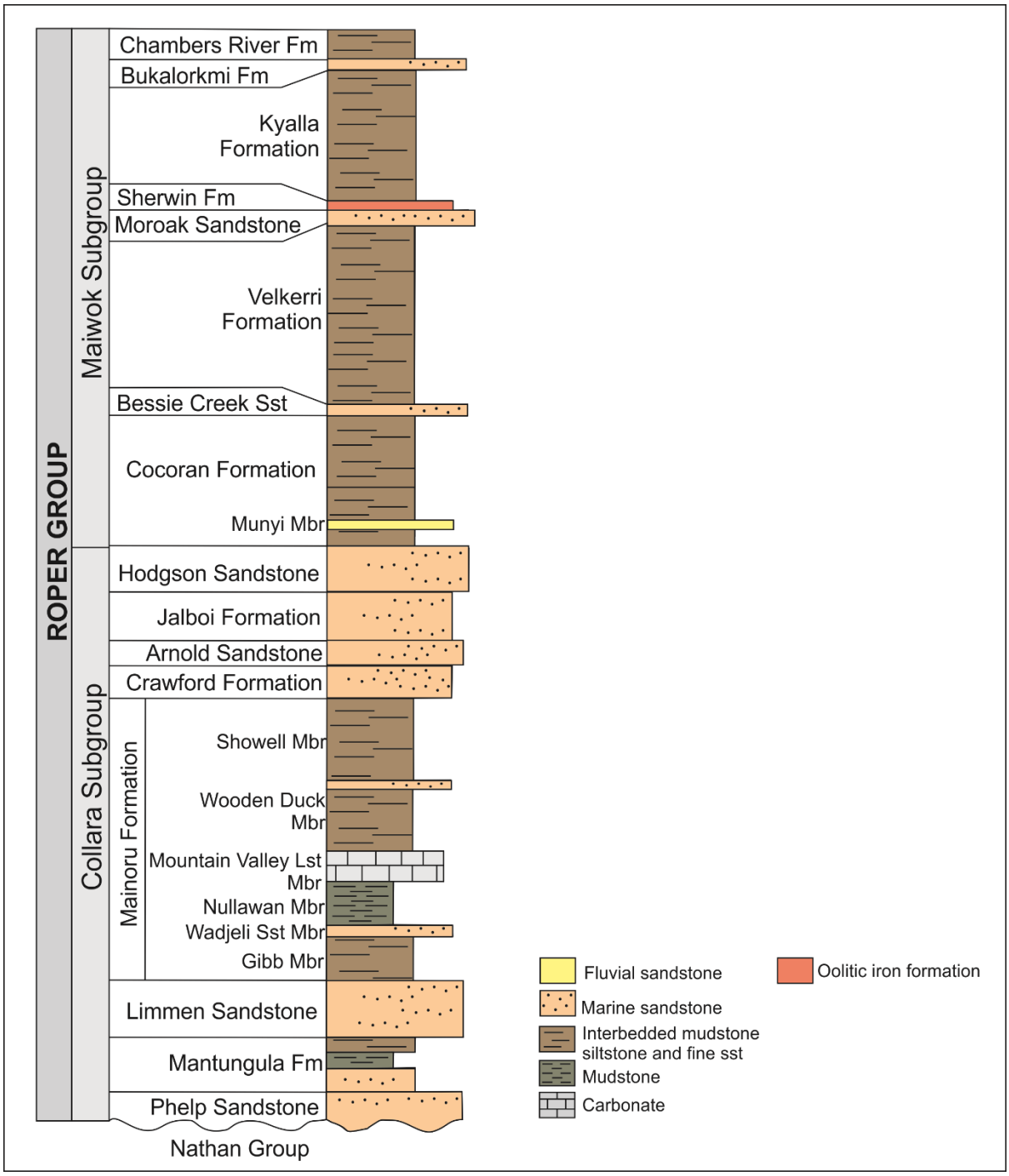

Figure 3: Generalised stratigraphy of the Roper Group from the Phelp Sandstone to the Chambers River Formation (lower to higher stratigraphy)

As for the geochronology of the Roper Group, the youngest single grain from Bessie Creek Sandstone has been used as the maximum depositional age constraint for the Maiwok Subgroup at 1386 ± 13 Ma (U–Pb zircon; Yang et al., 2018).

The minimum depositional age of the Roper Group is constrained by the Derim Derim Dolerite that intrudes the upper part of the succession. Abbott et al. (2001) reported an age of 1324 ± 4 Ma, from the Urapunga Region for the Derim Derim Dolerite, using secondary ionization mass spectrometry (SIMS) U-Pb baddeleyite. This is confirmed by Bodorkos et al. (2020) using isotope dilution thermal ionization mass spectrometry (ID-TIMS) on the same baddeleyite sample, with a reported age of 1327±0.6 Ma. Yang et al. (2020) obtained a younger ID-TIMS U-Pb baddeleyite age of 1312.9 ± 0.9 from a sample of the Derim Derim Dolerite collected from the northern Beetaloo Sub-basin around 200 km south of the Urapunga Region.

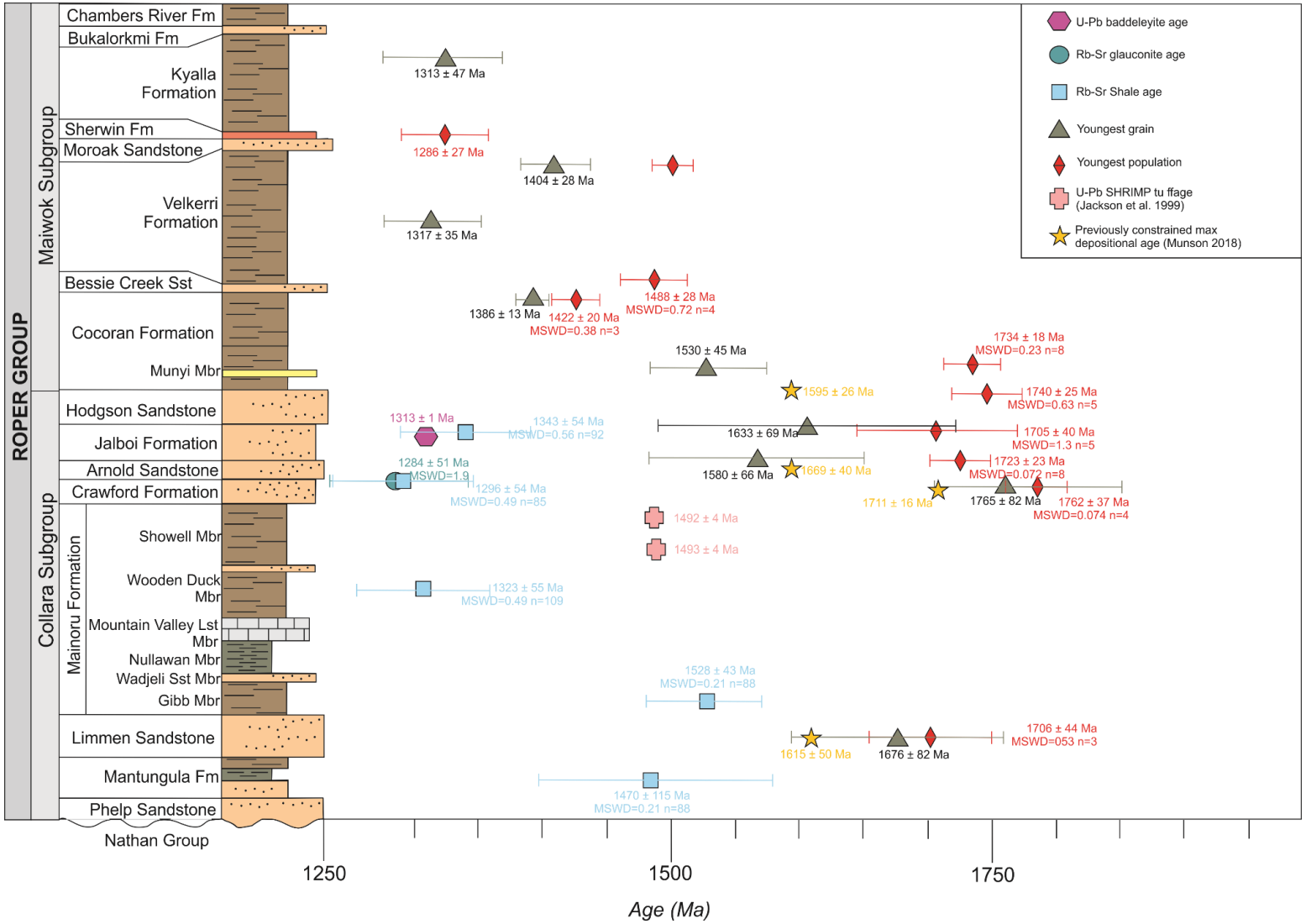

Figure 4: Generalised stratigraphy of the Roper Group from the Phelp Sandstone to the Chambers River Formation (lower to higher stratigraphy) with corresponding ages previously dated.

2.4. Velkerri Formation

Within the Roper Group is the Velkerri Formation. It is a black shale dominated unit that represents the initial relatively deep-water facies of a shoaling upward sequence. It comprises dominantly basinal facies transitioning up-section to cross-bedded sandstones of a high-energy, tide-dominated shoreline of the Moroak Sandstone (Abbott & Sweet, 2000; Munson, 2016). As for the geochronology of the Velkerri Formation, the black shales are constrained by a combination of absolute ages (Re–Os) and maximum depositional ages (U–Pb detrital zircons) to be between 1390 ± 10 Ma and 1360 ± 20 Ma (Kendall et al., 2009; Yang et al., 2018; Bodorkos et al., 2020).

There have been four prominent basin redox studies conducted on the Velkerri Formation, along with other Roper Group formation data, that suggest a redox structure for the basin. Firstly, Shen et al. (2003) characterised deep water anoxia along with oxygenated shallow waters based on iron speciation data. However, both Cox et al. (2016) and Mukherjee and Large (2016) used trace metals in shales and pyrite, respectively, to argue for oxygenated shallow waters, suboxic to anoxic deep waters, and intermittent euxinia.

The Velkerri Formation is divided into three lithostratigraphic members (Munson et al., 2018): the Kalala Member — interpreted to be a condensed transgressive system tract; the Amungee Member — comprising the primary black shale facies; and the Wyworrie Member (oldest to youngest).

The Amungee Member consists of thinly laminated, grey green to dark grey clays, pale grey siltstones, and the rare fine-grained sandstones. It is interpreted to have been deposited below storm-water wave base (Warren et al., 1998; Munson, 2016; Munson et

al., 2018; Sheridan et al., 2018). The organic enrichment within the Amungee Member occurs in three prominent horizons, informally referred to as the A, B, and C organofacies (oldest to youngest). These horizons show with no change in grainsize that correlate with the high TOC enrichment (Warren et al., 1998; Cox et al., 2016) and these horizons do not reflect changes in the energy of deposition or the water depth, but instead these intervals reflect changes in the water column biochemistry (Warren et al., 1998). The measured organic carbon isotope ratios ($\delta^{13}C_{org}$) from samples of the Amungee Member range between approximately 35‰ and 32‰ (Cox et al., 2016; Revie & Normington, 2020).

2.5. Drill Core Urapunga-4

This study focuses on the BMR Urapunga-4 drillhole, which was provided by Geoscience Australia drill core repository in Canberra. The drillhole is located in the Urapunga region (fig 1) at Latitude: 141˚ 32’ 17” S; Longitude: 134˚ 17’ 29” E and is one of three fully cored holes drilled as part of contract drilling program in 1985 to obtain a complete section of the Roper Group (Sweet & Jackson, 1986). Urapunga-4 represents the type-section of the Velkerri Formation (Crick et al., 1988; Crick, 1992; Summons et al., 1994; George & Ahmed, 2002).

2.6 Drill Core ELT002

The ELT002 drillhole was provided by BHP, it runs from 214m to 836m and is located at south McArthur Basin close to Beetaloo Sub-basin (fig. 1).

3. METHODS

LEGACY DATA

Existing data from Urapunga 4 are summarised in Appendix

A from Martin Kennedy's Australian Shale Carbon Sequestration group. Where relevant (i.e TOC) previous data were used in conjunction with newly collected data.

SAMPLE COLLECTION

Urapunga-4 sample collection used the previously collected chips and pre-crushed samples from Macquarie University, as well as new chips collected for this study. A total of 134 samples were used from the legacy data, and 29 samples were newly collected. The sample collection intervals are roughly every 3m, to ensure a representative sample-set through the core.

A total of 99 samples were collected from ELT002, these included two sandstone and 97 shales. Shales were collected roughly every 4m.

3.1 Sedimentology

A detailed stratigraphic log was recorded before sampling of the drill core. Characteristics logged were, grain size, shape, sorting, colour, sedimentary structures and notes. The detailed stratigraphic log was digitised using EasyCore software (Appendix H and I). Using lithostratigraphic technique, lithofacies were grouped based on grain size and sedimentary structures.

3.2 U–Pb dating.

Two sandstones were collected from the ELT002 drill core from the Beetaloo Sub-basin.

Sandstone core samples were crushed and milled, and the zircon grains were separated using panning, and heavy liquids (LST 2.85 + 0.02 g ml^{-1}). Individual grains were handpicked without preference to size, colour, or shape, and mounted in non-reactive epoxy resin. Cathodoluminescence (CL) images, showing zircon internal structures, were obtained using [Hitachi SU3800 scanning electron microscope (SEM) at Adelaide Microscopy, The University of Adelaide. Zircon U–Pb geochronological data were obtained using a RESOlution LR 193nm Excimer laser system and Agilent 7900x inductively coupled plasma-mass spectrometer (LA-ICP-MS) at Adelaide Microscopy. A 30μm spot size was used on the zircons and frequency of 5Hz at 65% intensity and an ablation period of 30 seconds. These data were collected in one analytical session spanning two days. GEMOC GJ-1 zircon was used as a primary standard to correct instrumental fractionation. The standard has a published, $^{207}Pb/^{206}Pb$ age of 607.7 ± 4.3 Ma, $^{206}Pb/^{238}U$ age of 600.7 ± 1.1 Ma and $^{207}Pb/^{235}U$ age of 602.0 ± 1.0 Ma (Jackson et al. 2004). The Plešovice zircon was used as an internal stand to assess the accuracy before and during the analysis of the unknowns, it has a published $^{206}Pb/^{238}U$ age of 337.13 ± 0.37 Ma (Sláma et al. 2008). The Plešovice zircon yields a weighted average mean of $^{206}Pb/^{238}U$ age of 339. 2 ± 1.1 (n=13, MSWD=1.2). Data was processed in the software package LADR 1.1.05 (Norris & Danyushevsky., 2018). A concordance of ≥90% in zircon analyses was decided to best represent the data using the calculation ($[^{206}Pb/^{238}U]/[^{207}Pb/^{206}Pb]*100$).

3.3 Rb–Sr dating

Laser analyses on samples and standards were carried out at Adelaide Microscopy, University of Adelaide using a laser ablation (RESOlution-LR ArF 193nm excimer laser) inductively couple-mass spectrometer (Agilent 8900x ICP-MS/MS) with the analytical parameters and tuning conditions following Redaa et al. (2022).

One spot analysis consisted of 20 seconds of gas background with 40 seconds of ablated signal. Strontium isotopes were measured in the oxidised molecule SrO. Strontium is oxidised with N_2O gas in the reaction chamber (e.g., $^{87}Sr^{16}O$ formed from ^{87}Sr at 103 amu), whilst the unreactive ^{85}Rb was measured on-mass. Dwell times for each SrO isotope were 50ms, 10ms for Rb and 5ms for all other masses totalling to 0.31 seconds.

In situ Rb–Sr dating of CRPG reference material Mica-MG prepared as a nano-powder pellet and a phlogopite mineral sample MDC, sourced from the same quarry in Bekily, Madagascar, were assumed to be of the same age and were used as primary and secondary standards respectively. Glass standards NIST-610 and BCR-2G were also analysed as standards for element quantification. Isochron ages were calculated using IsoplotR software and a Rb decay constant of 1.393 x10-11 was used.

The standards Mica-MG and MDC were anchored to its reported $^{87}Sr/^{86}Sr$ value of 0.72607 ± 0.00363. These gave an age of 520 ± 4 and 537 ± 13 Ma, respectively, within uncertainty of Mica-MG dated at 519 ± 7 Ma. Data for the secondary standard and all unknowns can be found in Appendix F and G.

3.4 Pyrolysis and Rock Eval

Samples of both drill cores were washed to be free of surface contamination and crushed to a fine powder in a tungsten carbide disk mill (samples include only newly collected samples from the Urapunga-4 and ELT002).

Powdered samples were weighed out ~80mg into crucibles. However, where samples did not look particularly organic rich, larger sample sizes (<130 mg). Samples were loaded onto a Weatherford Source Rock Analyser. The Weatherford SRA rock standard was used to at the beginning and end of each set (10 samples). An internal Adelaide Standards MCD005 was used every ten samples, to ensure replicability of data. TOC, S1, S2, Tmax, HI, OI and PI results for each sample were produced.

3.5 Elemental Analysis

A total of 102 samples from U4 and a total of 91 samples from ELT002 were weighted out for C% and C(org).

To determine C% and N%, within the sample, 0.4mg was weighted into a foil capsule and place into a PerkinElmer Series II CHNS/O EA-IRMS carousel. To obtain organic carbon ($\delta^{13}C_{org}$) isotope values, the shales were acidified to remove any inorganic carbonate fraction. This was performed by leaching a fraction (~1mg) of the powdered sample in vials with 10M HCl.

The supernate was then carefully poured off and the residue left to dry. These were repeatedly washed with DI water to ensure no acid remained. Using the weight difference, and total organic carbon values, it was possible to calculate the required sample size based on the individual sample's carbon content. The powdered samples were then weighed out into foil caps the caps and placed in a PerkinElmer Series II CHNS/O EA-IRMS carousel. Standards were analysed every 10 samples: Glycine, Glutamic, TPA. Glycine was used as the calibration standard.

4. OBSERVATIONS AND RESULTS

4.1 Sedimentology

Both Urapunga-4 and ELT002 were logged and divided into lithofacies. Below are detailed descriptions of each lithofacies. Urapunga-4 has been subdivided into 14 different lithofacies ranging from black siltstones to coarser sandstones. Overall, Urapunga-4 is a black shale dominated core. ELT002 has been subdivided into 19 different lithofacies and is defined by coarser grained lithologies, such as Facies I sandstones, in comparison to the Urapunga-4 core.

4.1.1 URAPUNGA-4

Facies A is characterised by a laminated black shale with centimetre scale interbedded siltstone and sandstone, lenticular bedding, irregular bedding, syneresis cracks, and minor slumps and convolute bedding. Facies B consists of fine to medium-grained sandstones that are thinly laminated (0.5cm scale), and contains mud rip-up clasts. Facies B1, a subset of facies B, consists of medium to coarse sand grains that are sulfide-rich. Facies C is a coarse-grained sandstone, which is quartz-rich (with minor lithics) and has subangular grains up to granule size. It has a sharp basal contact that is distinguished by a gravel beds. Facies C1 is a vuggy, granular, quartz-rich sandstone, however, unlike facies C, it has more rounded grains. It has some clay rip-ups, and is massive to weakly laminated. Facies D, previously identified as the Sherwin Ironstone, is an iron-rich sandstone that contains ooids, rare oxidised millimetre scale laminations, and mud rip-ups. Facies E is a broad lithostratigraphic facies defined by millimetre scale laminated shale that is interbedded with siltstone, and contains minor slumping and convolute bedding. Facies E1 is represented by a black shale that is similar to E but

is more massive. Facies E2 is a light grey siltstone that is weakly laminated with glauconitic beds (0.5 – 1cm thick). Facies E* is greener and less silty siltstone, with black laminations. Facies F is a porcelaneous, massive, grey-green, very fine-grained mudstone with minor laminations. Facies G is characterised by interbedded sandstone and siltstone with nodules. Facies H is a porcelaneous green shale. Finally, facies I is a tan, very fine-grained sandstone with some rip-up clasts and syn-sedimentary deformed beds. It is also distinguished by weakly laminated, medium to coarse-grained, feldspathic sandstones and granule layers with no distinct sedimentary structures.

4.1.2 ELT002

Facies A is a red mudstone–conglomerate with some quartz arenite clasts up to 15 cm diameter. This facies is fractured, making the original texture hard to determine. Similarly, facies B is also fractured. It is a mudstone with siltstone laminations and purple claystone interlaminations, interlayered with fine-grained, grey/purple sandstones. Facies B1, also broken up, is a millimetre to centimetre bedded, purple sandstone with grey siltstone interlayers. Facies B2 is very similar to B1, however, there are no interbeds present and the colour is pink/brown. Facies B3 is a fine to medium-grained sandstone with irregular laminations and occasional coarse sand to granular clasts. Facies B4 has more coarse-grained feldspars and sandy, wavy laminations with erosional bases. Facies B5 is a massive, medium to fine-grained sandstone with large, isolated feldspar clasts (<1.5 mm in size). Facies C is a massive siltstone and hematite-rich ironstone. Facies D is a massive, weakly laminated, coarse to medium-grained sandstone with common elongated mud rip-ups (up to 3 cm long). Facies D1 is characterised by a coarse-grained, feldspathic sandstone with centimetre scale bedding,

syneresis cracks, common cross-laminations interlayered with green shale, and occasional granule conglomerate layers with erosive bases. Facies D2 is a medium-grained arenite with centimetre scale bedding, faint laminations, occasional cross-beds, and light green porcelaneous silt/mud in syneresis cracks. Facies E is a hematite-stained, coarse-grained sub-arkose, with crossbedding and decimetre silt interbeds. Facies E1 is similar to facies E but has distinct millimetre hematite concretion. Facies F is a coarse-grained conglomerate with rounded clasts, which may include siderite and breccias. Facies G is defined by a millimetre to centimetre bedded, coarse-grained sandstone, with occasional irregular beds and interbeds of red siltstone to fine sandstone. Also, present are centimetre scale cross beds. There are also heavy mineral laminations, and occasional granule conglomerate beds. Facies G1 is represented by a medium-grained quartz-arenite with heavy mineral laminations, erosional bases, 1 cm scale cross-beds, and hematite granules/spots. Facies G2 is characterised by granule conglomerates interbedded with coarse-grained arenite and siltstone laminations. Facies H is a decimetre bedded, massive, fine-grained sandstone with slumping features, interbedded siltstone, and irregular bedding. Facies I is defined by a massive siltstone with occasional fine-grained sandstone lamination at centimetre scale.

4.2 Geochronology

4.2.1 U–PB IN ZIRCON

Sample ELT002-SST04 was collected from 295.1m – 296.0m. The other sample was taken from deeper in the well at 500m – 501m.

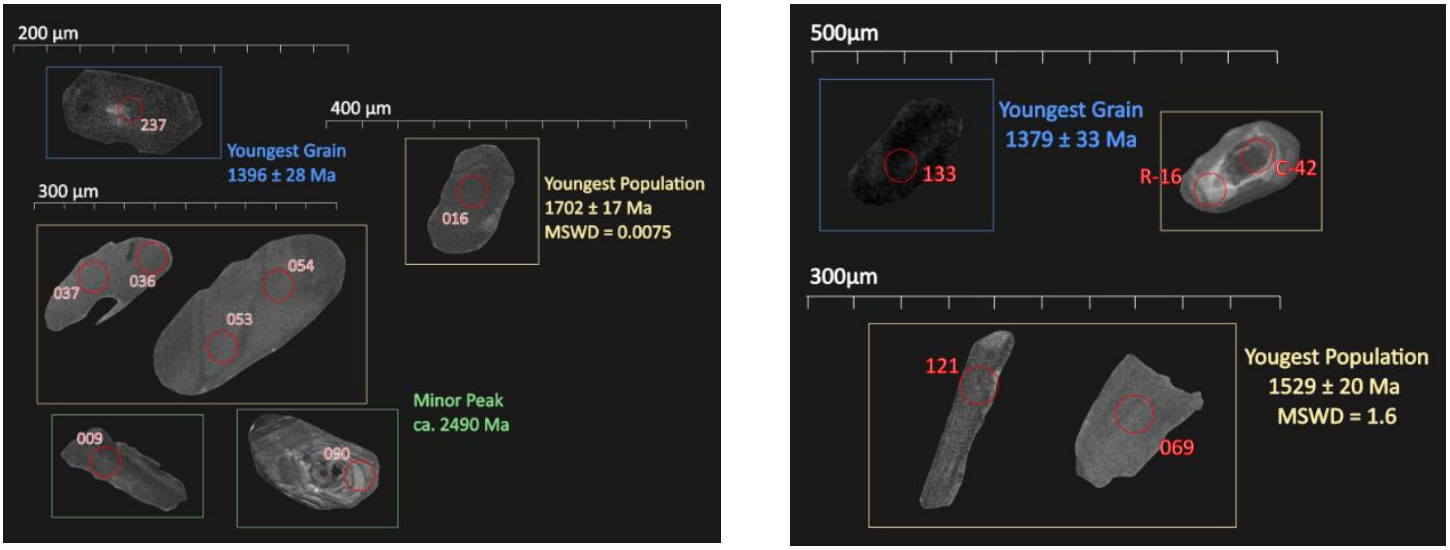

Figure 5: 207Pb/206Pb ages of the youngest populations and youngest single zircon grain. (a) on the left is sample ELT002-SST04 at 295.1-296m. (b) on the right is sample ELT002-SST08 at 500-501m

4.2.1(a) ELT002-SST04

A total of 243 grains were analysed from ELT002-SST04. Of these 37 were within 10% concordance (Fig. 7a).

These zircons have a $^{207}Pb/^{206}Pb$ age between ca. 2506 Ma and 1396 Ma. Data form a major peak at ca. 1757 Ma and minor peak at ca. 2490 Ma. (Fig 7). The youngest near concordant zircon yields a $^{207}Pb/^{206}Pb$ age 1396 ± 28 Ma (concordance = 93%). The caveat to this youngest near concordant zircon it has a concordance of 93%, where the next youngest concordant zircon is 1530 ± 43 Ma (concordance=95%). This suggests that this age must be treated with caution in case of contamination or Pb-loss.

The youngest population gives a weighted average of 1702 ± 17 Ma (MSWD =0.0075, N = 3). This is not within uncertainty of the younger grains within this sample and does not provide a good estimate of the maximum depositional age. Therefore, the YSG (youngest single grain), 1396 ± 28 Ma (93%) is tentatively suggested to represent the best estimate for the maximum depositional age.

4.2.1(b) ELT002-SST08

A total of 212 grains were analysed from ELT002-SST08. Of these 103 were within 10% of concordance (Fig. 7b). These zircons have a $^{207}Pb/^{206}Pb$ age range between ca. 2500 Ma and 1380 Ma (Fig. 6).

The youngest near concordant zircon yields a $^{207}Pb/^{206}Pb$ age of 1379 ± 33 Ma (97%). The youngest population gives a weighted average of 1529 ± 20 Ma (MSWD = 1.6, N = 3). Though these are out of uncertainty of each other, it is interpreted that the YSG (youngest single grain) represents the best estimate for the maximum depositional age.

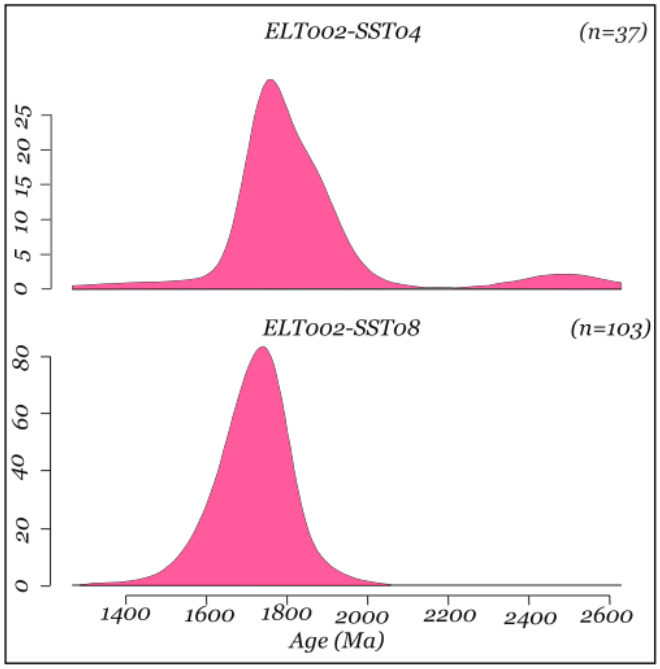

Figure 6: Kernel density estimate plots for ELT002-SST04 and ELT002-SST08

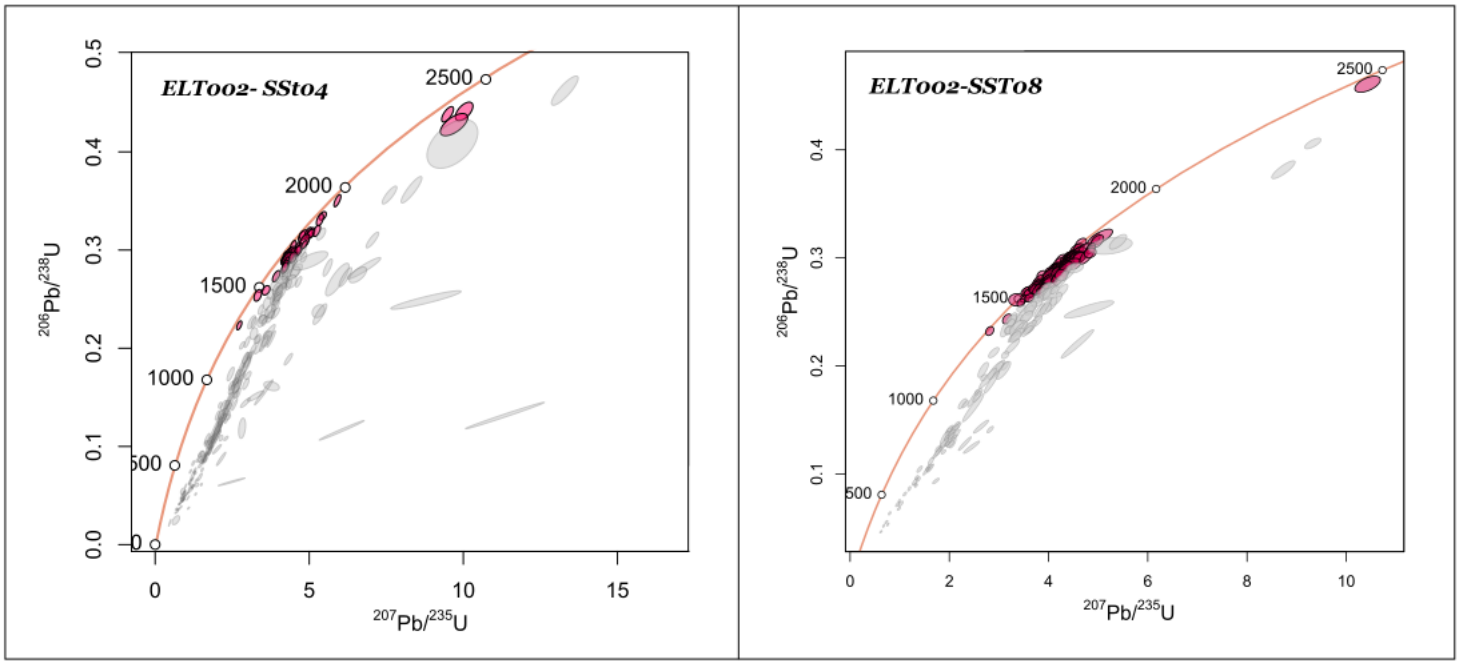

Figure 7: Concordance plot for (a) ELT002-SST04 (one data point excluded from concordia, due to common Pb). And (b) ELT002-SST08. Pink ellipses represent data that is within 10% of concordance and the grey ellipses represent the discordant data.

4.2.2 Rb–Sr dating of shales

Shales were analysed using the in-situ laser ICP-Ms/Ms technique, to establish a minimum depositional age of these rocks. The data were triaged using the method from Subarkah et al. (2022). A total of two hales were analysed from ELT002.

ELT002

Two samples were selected from ELT002 for Rb–Sr analysis at depths of 663.6m and 807m. These samples were selected as they had low detrital material, where it is most likely authigenic clays.

A total of 151 spots were analysed, and sample number ELT002_119 (663.6m) yielded an isochron age of 1330 ± 58 Ma (MSWD = 1.4). These data yielded a Sr^{87}/Sr^{86} initial

value of 0.7054. Sample number ELT002_807 (807m) yielded an isochron age of 1395 ± 41 Ma (MSWD = 1.3). These data yielded a Sr^{87}/Sr^{86} initial value of 0.7039. (Fig 8). These two isochron ages are within uncertainty of each other and give Sr^{87}/Sr^{86} initial ratios that are within the range of seawater during the Mesoproterozoic (Chen et al., 2022).

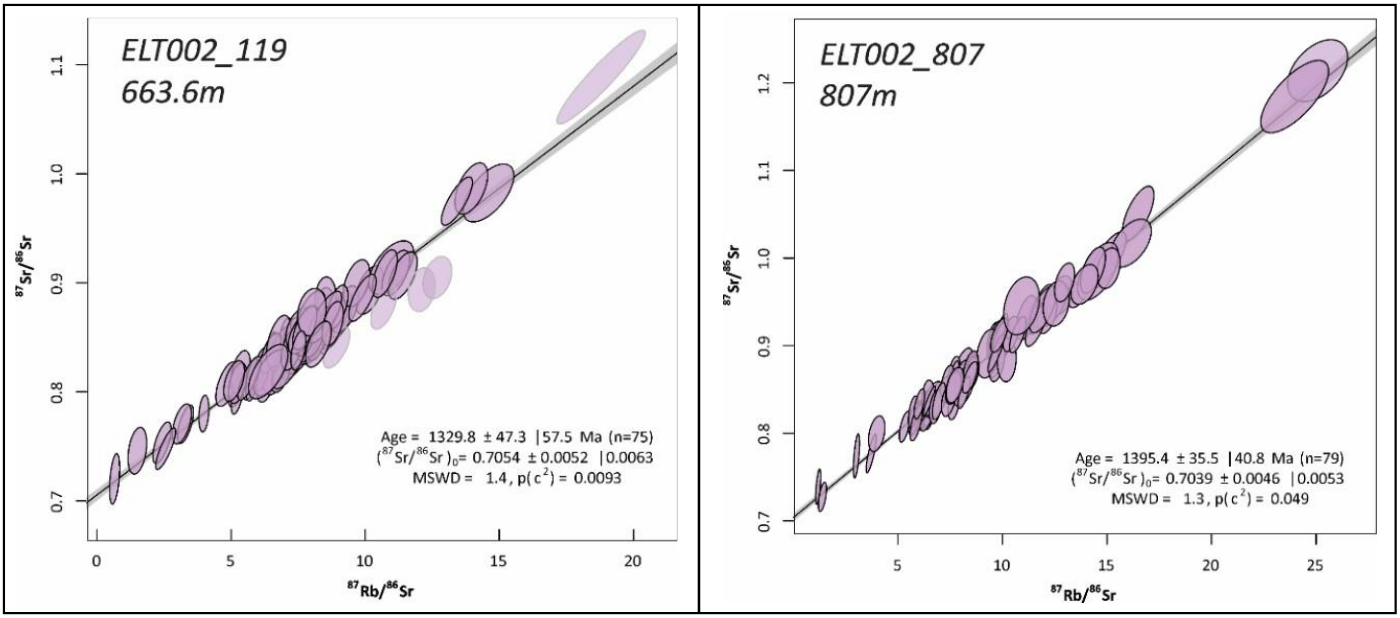

Figure 8: Calculated isochrons from(a) ELT002_119 at 663.6m, and (b) ELT002_807 at 807m. Ellipses without outlines are datapoints that have been excluded from the calculated isochron ages

4.3 Organic Geochemistry

TOTAL ORGANIC CARBON (TOC) AND C(ORG)

Samples from both ELT002 and Urapunga-4 were analysed for both TOC and organic carbon isotopes. Total organic carbon is used as a proxy for organic matter present in the sediment and is used as an indicator of the source richness with respect to how much hydrocarbon the sediment may generate (Rullkötter, 2003). Organic carbon isotopes are a representation of a small portion of the marine carbon cycle. Atmospheric carbon enters the ocean and exists in equilibrium with bioavailable HCO^{3-} and becomes a part

of the dissolved inorganic carbon pool. Organic carbon preferentially takes up light carbon leaving the pool isotopically heavy. The measurement of $\delta^{13}C_{(org)}$ is bulk organic matter, which can be a combination of two main sources: one being authigenic organic matter synthesised by primary producers in the ocean and detrital organic matter from continental weathering (Johnston et al., 2012).

4.3.1 ELT002

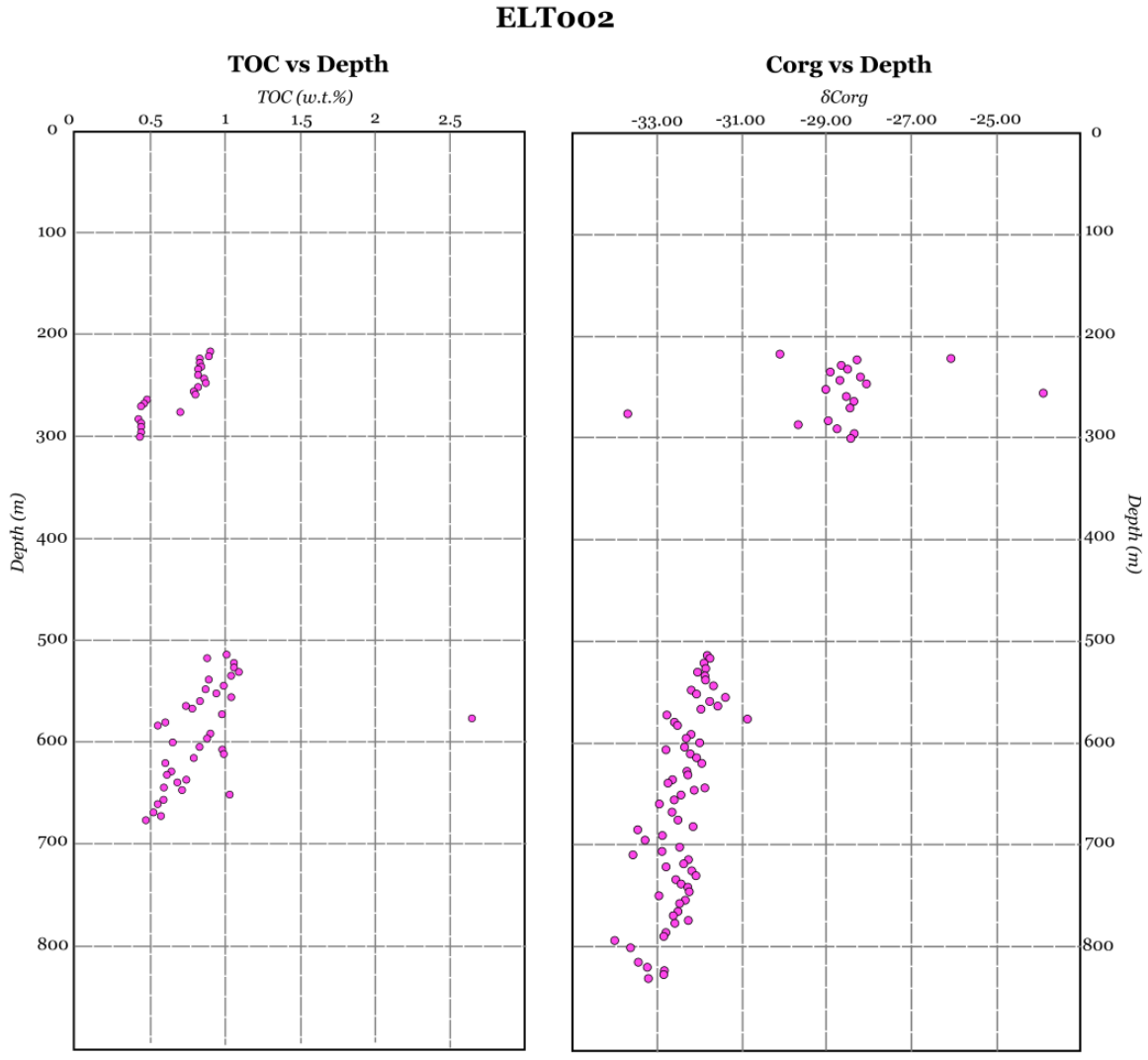

Figure 9: ELT002 (a) TOC vs Depth, and (b) δ13C(org) vs Depth

A total of 60 samples were analysed for TOC for the ELT002 core (Fig. 9a). Over the 500m TOC values range from 0.42 at 283.6m to 2.65 at 576.8 m. This high TOC value is an outlier and is treated with caution. The next highest value is 1.09 w.t% at 531.3m. The data show two distinct negative trends at 217.5 m – 300.9 m and 514.4 m – 676.7 m, respectively. Notably, there is also a stepwise shift (at 259.6 m; 0.8 wt%) to more negative values (0.48 wt%).

A total of 91 samples were analysed for $\delta^{13}C_{(org)}$ for the ELT002 core. Over the 500m $\delta^{13}C_{(org)}$ values range from -33.99 at 794.9m to -28.07 at 224.8m, however there are two outliers, -23.9 at 256.8m, and -26.07 at 221.8m. There is a general negative trend with depth. Though tenuous, there are 3 peaks -30.86 (576.8 m), -31.87 (644.8 m), and -32.09 (731.7 m), respectively.

4.3.2 Urapunga-4

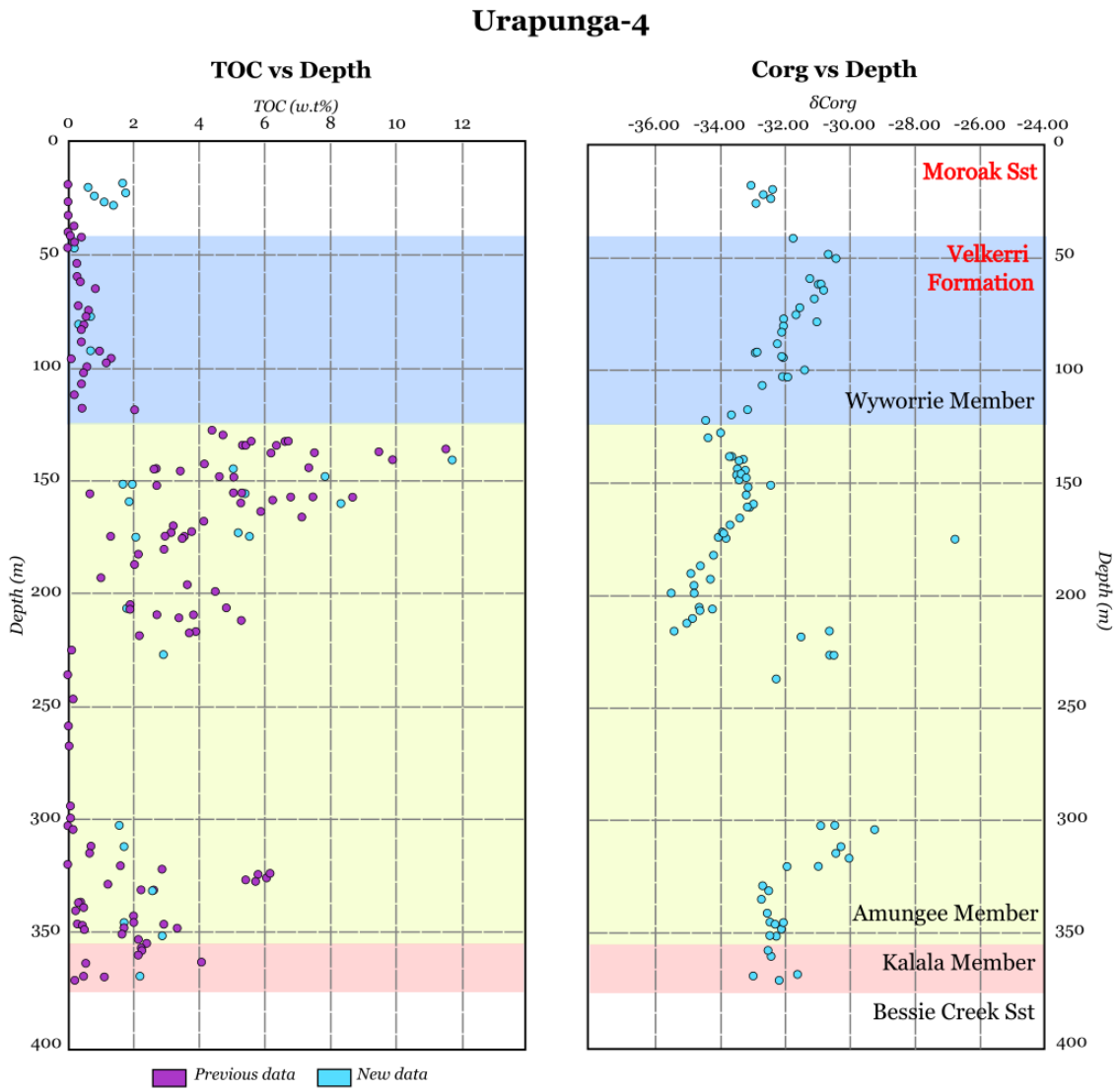

Figure 10: Urapunga-4 (a) TOC vs Depth, and (b) δ13C(org) vs Depth

A total of 71 samples were analysed for TOC for Urapunga-4, and a total of 129 samples that were previously analysed by Martin Kennedy's Australian Shale Carbon Sequestration group were added as additional data (fig. 10). The new data have a minimum value at 0.18 w.t % and maximum value of 11.7 w.t % (fig 10a). When complied with previously collected data, there are three main peaks in the data within the Amungee Member, from 118–187 m, 187–226 m, and 307.7–339 m.

From 28 m to 117.85 m there is a positive trend with depth. There are two intervals of higher TOC between 117.8 m and 225.03 m, reaching values of 11.7 wt % and 5.28 wt %, respectively. An obvious decrease in the TOC values follows this organofacies (until 304.52m), whereby TOC values are very low (X–X). However, this sharply increases again with a final interval of high TOC values, reaching up to 6.16 wt% (304.52m –339 m).

A total of 102 samples were analysed for $\delta^{13}C_{(org)}$ for Urapunga-4 (fig. 10b). There are two minimum values -88.5 and -54.17 ‰, however, they appear to be outliers and will not be included in the results. The $\delta^{13}C_{(org)}$ within the Urapunga-4 core have a range between -35.51 and -26.79 ‰. Generally, there is shift towards heavier $\delta^{13}C_{(org)}$ down section (~18.2 and 50.65 m), with a distinct shift towards lighter (more positive) values at 216.36 m. The main positive anomalies in the data are at 151.5 m, 175.5 m, 226.98 m, 304.52 m (-32.44, -26.79, -30.49, -29.24 ‰respectively). The main negative anomalies are at 92.6 m, 122.9 m, 199.2 m (-32.92, -34.45, -35.51‰ respectively).

5. DISCUSSION

5.1 What is the depositional environment of rocks in ELT002 and Urapunga-4?

5.1.1 ELT002

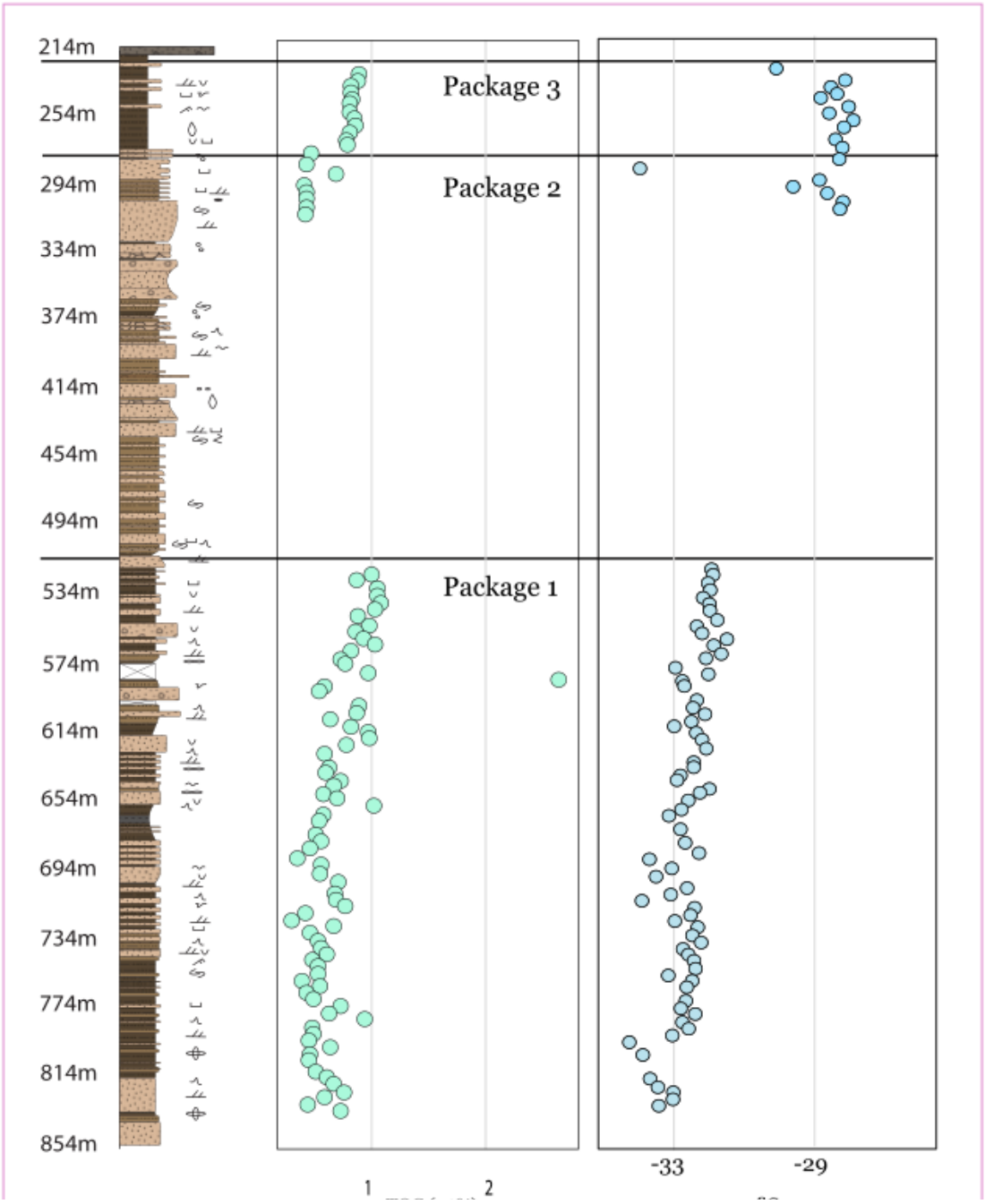

Figure 11: Genralised stratigraphy log of ELT002 with TOC and δ13C(org) values.

ELT002 has been divided into three main packages logged in the core, The first package, spanning from 512m to 854m (bottom of the core), exhibits significantly lower sand content compared to the overlying package. It is interpreted as a tide-dominated delta. The upper section of this package, up to 654m, displays desiccation cracks and lenticular (heterolithic) bedding, indicative of an intertidal zone that experienced periods of exposure. In contrast, the lower section of this package shows syneresis cracks, suggesting deposition in a subaqueous environment (Boyd et al., 1992). Given the interpretation of tidal dominance and observed sedimentary features, it is inferred that these fine-grained deposits represent tidal flats surrounding distributary channels of a delta system. Therefore, any coarse material in this package can be interpreted as channel fill deposits. In the corresponding geochemical data, drops in TOC values are observed, likely due to the inundation of sediment. Soft sediment deformation primarily occurs in the sands of this package, likely indicating rapid deposition (Boyd et al., 1992). This contrasts with the package above, where soft sediment deformation primarily occurs in the shales and suggests deposition from gravity flows. Therefore, any coarse material in this package can be interpreted as channel fill deposits. Overall, this package indicates a shallowing-up trend, transitioning from a subtidal delta front environment to an intertidal delta plain setting.

The second package in the core, spanning from 270m to 512m, consists of finer grained silts at the base and progressively sandier towards the top. The base of this package consists of siltstones with soft sediment deformation, while the top consists of channel sands. This package is interpreted as part of a river delta influenced with significant fluvial influence and evidence for tidal and wave processes (Boyd et al., 1992). This package exhibits classic features of distributary channels, including common scour and

fill structures, which suggest high energy conditions close to the delta mouth. The presence of soft sediment deformation in the siltstone beds of this package, may indicate gravity flow processes as part of a pro-delta fan deposit. The presences of syneresis cracks provide further evidence of a deltaic environment as they result from salinity changes facilitated by the mixing of freshwater (fluvial) and salt water (marine) sources, which would occur in river delta setting (Boyd et al., 1992). Apart from a noted drop in TOC at the top of this package, the rest appears to have been swamped with sediments, resulting in minimal shales and therefore a lack of geochemical data for this package.

The next package, located at the top of the core (from 216m to 270m (Facies B, B2)). It contains laminated shales, with occasional cross laminations, and ripple beds. These features are interpreted to be part of a quiet pro-delta zone below wave base. The core transitions into the much sandier package (described above), representing fining upwards sequences. The base of the shale at the transition to the sandier package is interpreted to be a parasequence boundary, or more specifically a minor flooding surface. Thus, it represents a considerable shift in water depth, which is reflected in the geochemistry, where a step down in TOC and $\delta^{13}C_{(org)}$ can be observed (fig. 11).

The overall palaeoenvironmental interpretation for this core is a succession of prograding deltaic parasequences. The stacking of these progradational packages reflects a larger regressive system, where base level dropped, and the continent extended basinward.

5.1.2 URAPUNGA-4

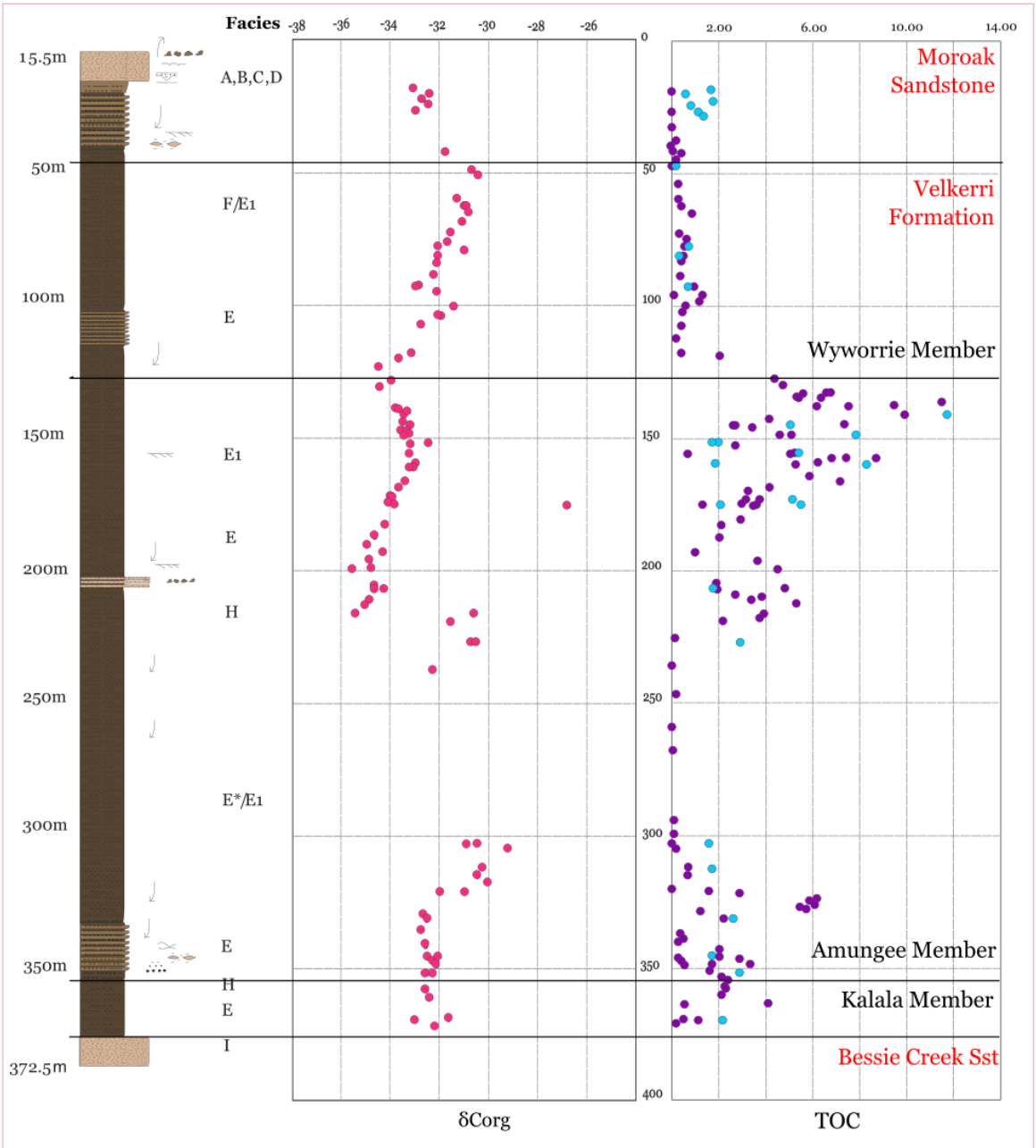

Figure 12: Genralised stratigraphy log of Urapunga-4 with TOC and δ13C(org) values.

The Urapunga-4 core comprises a sandstone unit at the top (Moroak Sandstone) and at the bottom (Bessie Creek Sandstone), separated by a predominantly black fine-grained unit, known as the Velkerri Formation. This formation consists of mudrock, siltstone, and minor sandstone. The lower portion of the Velkerri Formation exhibits a sharp

contact between the underlying sandstone of the Bessie Creek Sandstone, while the upper portion exhibits a coarsening upward trend towards the Moroak Sandstone.

The presence of glauconite in the Aumngee Member indicates a low-energy, off-shore marine depositional environment. According to Powell et al. (1987), most of the formation resulted from periodic turbidity currents, indicating gravity flow deposition on the continental slope. The middle of the Velkerri Formation represents the most distal environment, due to the higher proportion of claystone to siltstone and sandstone. These were likely deposited on an outer shelf to slope setting, affected by periodic tectonic activity that produced abundant slump bedding and work done by Schieber et al. (2018) interpreted that the sediments of the Velkerri were deposited by bed loads. The presence of cross-laminated sandstone, siltstone and claystone, graded siltstone, and occasional scours are additional evidence for periodic or irregular current reworking. There is a formation boundary at 42m into the Moroak Sandstone, a shift to a more proximal deltaic environment. This indicates shallowing and increased sediment input due to continental/deltaic progradation.

If the two cores were deposited concurrently, the observed palaeoenvironmental differences could represent lateral variations within the same depositional system (i.e. proximity to coastline, sediment supply, deltaic processes etc.). This is a reasonable interpretation given the considerable distance between these two cores (fig. 11 and 12). Conversely, if the two cores were deposited at different times, the palaeoenvironmental disparities might signify changes in the depositional system through time. Dating of the

ELT002 core is important to understand which of these two scenarios detailed above is true.

5.2 What process led to organic enrichment in the Upper Roper Group of ELT002 and Urapunga-4?

The geochemical proxies used to help understand the organic enrichment within the Velkerri Formation are total organic carbon (fig. 10a) and $\delta^{13}C_{(org)}$ isotopes (fig 10b). TOC is the measure of organic carbon present in the source rock. However, it should be treated with caution as it is sensitive to maturity and often decreases as hydrocarbons are expelled (Daly & Edman, 1987).

Carbon isotopes are preserved in shales through the process of organic life in the water column dying. The amount of carbon isotopes in the shale is determined by how much life was present in the water column. If there is a lot of organisms in the water column, and life preferentially takes up light carbon isotopes, the water will become depleted in ^{12}C, then because the water is so depleted in ^{12}C then life will resort to taking up ^{13}C. Therefore, there will be an increase in mass of $\delta^{13}C_{(org)}$ that follows the inorganic C isotope trend, but much lighter (highly negative), because this is measuring the isotopic trend in the organic remains of the organisms, not the remaining water. This then provides a chemical proxy for the amount of productivity occurring in the water column.

Shales containing high levels of total organic carbon result from either the efficient export and burial of organic matter, low rates of sedimentation, or a combination of the two. The preservation of organic matter is influenced by the degree of remineralisation, which is dependent on the duration of oxygen exposure and the overall burial rate in the sediment. These processes, in turn, are influenced by various factors, including the

oxidising capacity of the water and sediment columns, sedimentation rates, and the clay mineralogy of the sediment (Canfield, 1994; Hedges and Keil, 1995; Kennedy et al., 2002; Tosca et al., 2010; Hemingway et al., 2019).

These two geochemical proxies can be used to better understand why fluctuations in TOC occur. If it is due to productivity fluctuating, in which case TOC and $\delta^{13}C_{(org)}$ will correlate or is it due to varying amounts of siliciclastic sediment input, in which case TOC varies, but $\delta^{13}C_{(org)}$ does not.

5.2.1 ELT002

When interpreting the depositional environment of the ELT002 core (Fig.11), it appears that fluctuation within the core may not necessarily attributed to changes in productivity but rather variations in detrital input where drops in TOC are observed, they correspond to sandy intervals indicating that it is likely due to sediment swamping. However, when TOC is plotted against $\delta^{13}C_{(org)}$ there is an interesting distribution. The shallow data points will not be considered in the interpretations as the pyrograms for these samples show there is no S2 peak, which is the organic carbon, and what little TOC there is in these samples is in the S1 peak (freed carbon) fraction.

As for the deeper samples (fig. 13b), there is a very slight positive correlation between TOC and $\delta^{13}C_{(org)}$, this either suggests that the increase in TOC is due to an increase in productivity, rather than change due to sea-level change and different rates of sedimentation (Cox et al., 2016, 2022), or this reflects a general trend with increasing maturity (Daly & Edman, 1987). To determine which of these interpretations is accurate, further research is warranted.

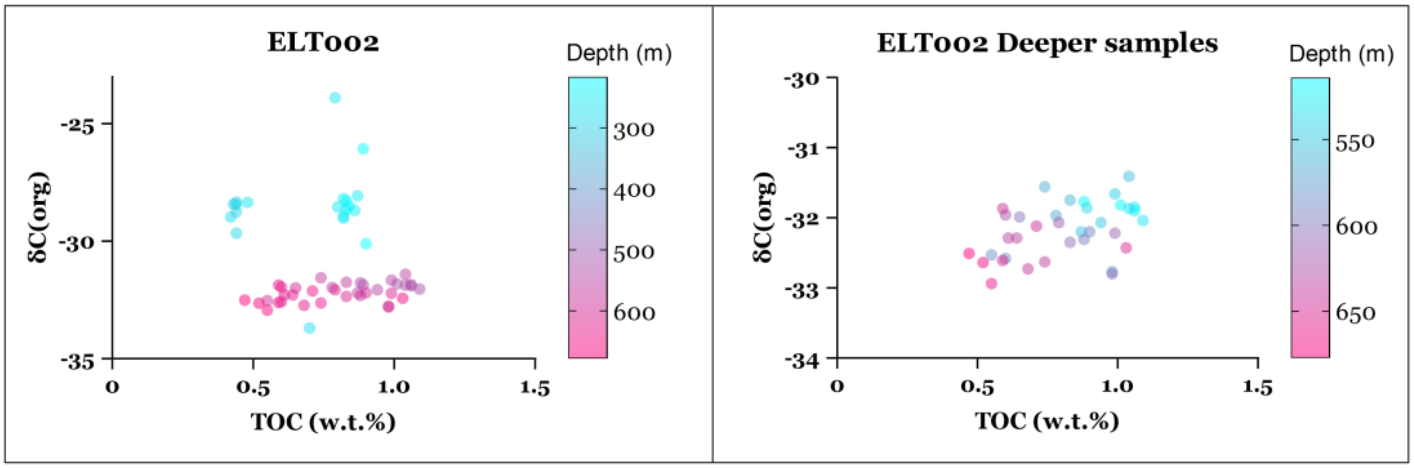

Figure 13: (a) ELT002 all data $\delta^{13}C_{(org)}$) vs TOC against depth (m) and (b) ELT002 only the deeper samples $\delta^{13}C_{(org)}$) vs TOC against depth (m).

5.2.2 URAPUNGA-4

As for the geochemistry associated with Urapunga-4, there are three shales with high organofacies within the Amungee Member. The A shale, positioned at the base (depths) of the Amungee Member, exhibits a peak in TOC (6 w.t %), followed by a negative trend in TOC values and corresponding positive trend in $\delta^{13}C_{(org)}$ (from -32‰ to -29‰) up-section (fig. 12). This shift in $\delta^{13}C_{(org)}$ is suggested to be the result of increased primary production into the offshore environment.

Strangely, in figure 14, the A shale shows a negative relationship between TOC and $\delta^{13}C_{(org)}$ indicating sediment influx. This is an increase in $\delta^{13}C_{(org)}$ with depth as TOC is decreasing. This must mean that sediment supply is outpacing the increased carbon production, therefore, sediment is swamping organic matter.

In the B shale, there is a positive correlation between $\delta^{13}C_{(org)}$ and TOC, where values increase from 2 w.t % to 5.8 w.t % and -32‰ to -30‰, respectively. This indicates increased primary productivity and likely more favourable conditions for life. However, following these high values, there is an abrupt shift to more negative (lighter) $\delta^{13}C_{(org)}$ values, while TOC values remain high. This shift may be attributed to an influx of sediment, aligning with the deposition of a sandy unit at this horizon. The source of this coarse sediment into the distal marine environment could be a consequence of a storm event or period of increased continental sediment output. This interpretation is also supported by TOC vs $\delta^{13}C_{(org)}$ (fig.14), where the B shale show a little positive $\delta^{13}C_{(org)}$ increase with increased TOC, therefore indicating the possibility of a small organic bloom immediately followed by increased sediment input, possibly from a storm event.

In the C shale, $\delta^{13}C_{(org)}$ values increase up-section from -36‰ to -32‰, which corresponds with increasing TOC values (1 w.t % to 11 w.t %). Like the positive correlation recorded in the base of the B shale this likely reflects increased primary productivity. In the TOC vs $\delta^{13}C_{(org)}$ figure (fig.14), the relationship is hard to see but there appears to be an increase in TOC and an increase in $\delta^{13}C_{(org)}$ contributing to interpretation from geochemistry vs depth.

In the Wyworrie Member, low TOC values coincide with a positive trend in $\delta^{13}C_{(org)}$ values. This could suggest that the increased primary productivity was not preserved in the shale geochemistry. This relationship is observed in fig.14 and is similar to the A Shale, where the Wyworrie Member shows a negative relationship where decrease in $\delta^{13}C_{(org)}$ values with depth. This could be due to life doing so well that even though there is a lot of life (increasing $\delta^{13}C_{(org)}$) the organic build up is swamped by even more clastics from a prograding delta, that is bringing in lots of nutrients for life to bloom but swamping it with sediments.

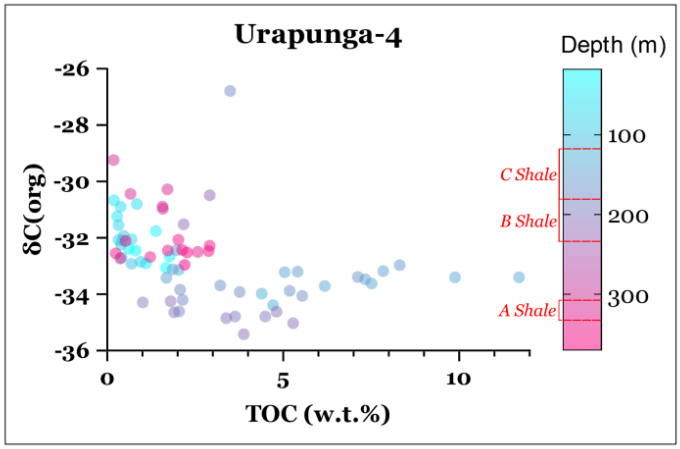

Figure 14: Urapunga-4 $\delta^{13}C_{(org)}$) vs TOC against depth (m), highlighted A, B, and C Shale

5.3 What is the age of the rocks in ELT002? And what is their provenance?

The maximum depositional age for the sediments within ELT002 is constrained by the youngest detrital zircon, implying that the sediment must be younger than this age. Data in this study shows that the maximum depositional age is 1379 ± 33 Ma. This is broadly supported by the youngest zircon in ELT002-04, which yields an age of 1396 ± 28 Ma. Rb-Sr age constrains the minimum depositional age because the illite that is being dated in the shale is interpreted to have formed authigenically, or during early diagenesis (the

initial ratio being close to seawater supports this as it suggests that the illite records sea water Sr values that have not been reset by more radiogenic waters). The caveat to this is that if there were lots of detrital illite, then it would yield n greater age. Fortunately, detrital illite is much rarer in the Proterozoic (Rafiei & Kennedy, 2019; Rafiei et al., 2020), this is because soils had not evolved, and most detrital clay minerals are formed in soils. Therefore, the minimum depositional age is 1395 ± 41 Ma (ELT002-807; MSWD = 1.3) with an initial Sr ratio of 0.7039 (fig. 8), which overlap with the expected values of Mesoproterozoic seawater that also supports this reflecting clay mineral growth on, or close to the seafloor. Therefore, Rb-Sr ages likely reflect actual depositional ages as they also sit comfortably within the errors of the maximum depositional ages of zircon U-Pb data. However, from this data the age window for deposition of ELT002 is 1412 Ma to 1354 Ma as seen in fig 15.

Previous geochronological work on the formations within the greater McArthur Basin can help to decipher the unknown formation in ELT002. The Velkerri and Kyalla Formations are sedimentologically and geochronologically most similar to those observed in ELT002. Various attempts have been made to date the Velkerri Formation, with Re-Os ages of 1417 ± 29 Ma, 1361 ± 21 Ma, and 1390 ± 10 Ma, as well as a young detrital zircon grain (1308 ± 41 Ma) found in Yang et al. (2018) (Kendall et al., 2009; Yang et al., 2018; Bordorkos et al., 2020). Additionally, Subarkah et al. (2022) determined an age for the Velkerri Formation 1434 ± 19 Ma, using Rb-Sr in shales. Crombez et al. (2023), suggests that the Velkerri Formation was likely deposited between ca.1420 and 1300 Ma and the overlying Kyalla Formation between ca. 1270 to 1210 Ma. However, both the Velkerri and Kyalla formations are intruded by the Derim

Derim Dolerite as sills that are dated at 1324 to 1313 Ma (Munson, 2016; Abbott et al., 2001; Nixon et al., 2022; Yang et al., 2019), implying the age ranges outlined by Crombez et al. (2023) are too young. Crombez et al. (2023) suggests that the intrusive ages are derived from out-cropping units, with poor constraints on their stratigraphic position. However, the Derim Derim is now dated in many places, even where it cuts the Kyalla in drill core (Nixon et al., 2022). The evidence suggests that the Derim Derim Dolerite intrudes both the Velkerri and Kyalla Formation, therefore ca. 1313 Ma is the best minimum depositional age for the Kyalla and Velkerri Formation.

As stated above, the absolute minimum depositional age is ca. 1313 Ma for the Velkerri and Kyalla Formation. The two standard deviation error windows for the lower succession in the ELT002 just overlap with the permissive age of the Velkerri Formation. However, it much more firmly overlaps with the age of the Kyalla formation. The difference in sedimentology between the rocks in ELT002 and the Urapunga well (and other Velkerri formation descriptions in the literature) suggests that here I have dated the Kyalla Formation. This is the first time this formation has been directly dated.

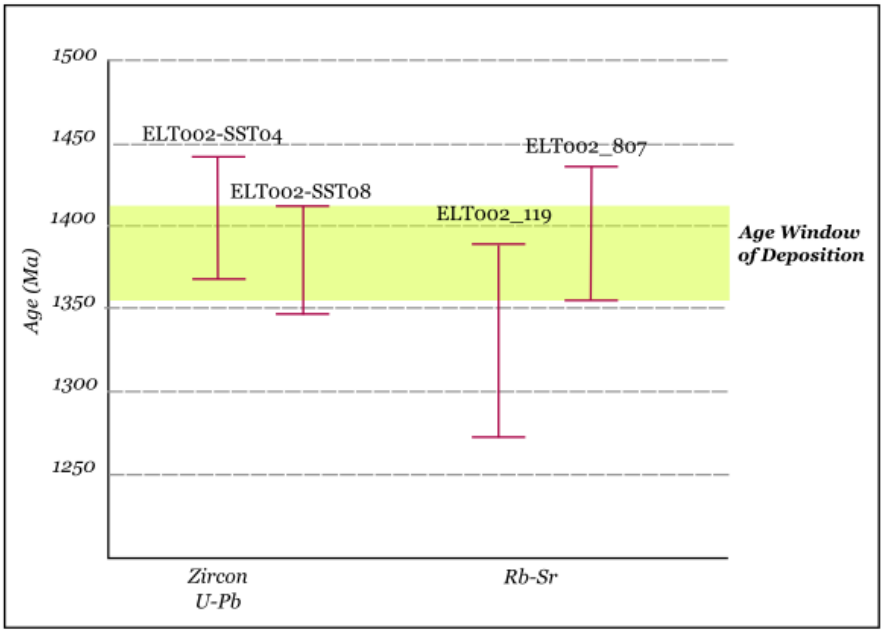

Figure 15: Age Window of deposition for the ELT002 core.

In an attempt to constrain the possible source regions of the zircons within the sandstones of ELT002, data were plotted on a multidimensional dimensional scaling plot (MDS). MDS is a statistical technique that quantifies and visualises the degree of dissimilarity among geochronologic samples (Vermeersch, 2013; Sharman et al., 2018). Where the degree of dissimilarity is visualised by the plotted distance between individual samples. These plots are an easy way of visualising large amounts of data and where samples plot closer together it can be interpreted that they are more similar in their detrital spectra and vice versa. The MDS plot (fig 16) was generated using detritalPy (Sharman et al., 2018). Data from surrounding similar aged or older terranes were also plotted, highlighting variations in source regions for different parts of the basin and at different times.

This study's samples, ELT002-SST04 and ELT002-SST08, were plotted along with ELT002-06 (a sample not included in this study but was collected from 305m in

ELT002) on an MDS plot (fig. 16). Yang et al. 2020, proposed a bathymetric high in the Daly Waters region which separated the sediments of the Birrindudu Basin from those within the McArthur Basin and Beetaloo Sub-basin, as seen in Fig 16, forming two distinct clusters. The samples from ELT002 plot on the right side of the figure, closer to the Roper Group (McArthur Basin and Beetaloo Sub-basin) samples, further away from where the Tijunna and Bullita Groups (Birrindudu Basin) plot.

Within the Roper Group formations, the ELT002 samples plot closer to the Kyalla Formation, Bessie Creek Sandstone, and the Moroak Sandstone compared to the Velkerri Formation. Yang et al. (2018, 2019, 2020) found there was a shift in provenance in the Maiwok Subgroup. Detrital zircon U-Pb and Hf data suggested that formations in the lower parts of the subgroup (Bessie Creek Sandstone, Velkerri Formation, and Moroak Sandstone) were sourced from southeasterly and easterly sources (Mount Isa Region, Coen-Georgetown region and SAC), whereas the Kyalla Formation at the top of the Maiwok Subgroup received detritus from the Aileron Province to the South of the basin.

The ELT002 sands reveal broad detrital peaks ca. 1750 Ma, with little preservation of much younger detritus. The age is fairly prevalent in the North Australian Craton (NAC) sediments. The Aileron Province and Tanami, located south of the Tomkinson Province, are distinctly marked by younger magmatic and metamorphic events (< ca. 1810 Ma (Howlett et al., 2015)), when compared to other regions within the NAC. These events include the Stafford Event (1810-1790 Ma), the Yamba Event (ca. 1790-1770 Ma, with the CAT Suite at ca. 1773-1750 Ma), the Strangways Event (1740-1690 Ma), the possible Leibig Orogeny (ca. 1640 Ma), and the Chewings Event (1590-1550

Ma) (Claoué-Long et al., 2008, Collins & Williams, 1995, Dirks & Wilson, 1990, Scrimgeour et al., 2005b, Howlett et al. 2013, Claoué-Long & Hoatson, 2005). Notably, the Stafford Event is defined by large amounts of magmatism and is considered a potential source for the prominent peak observed in these samples (Howlett et al., 2015). The alternative is that these are recycling older basin sediments, which are also dominated by these peaks, however this is much harder to ascertain.

Yang et al. (2018, 2019, 2020) suggested that this shift to southerly sources may have been related to a closure of the ocean that separated the combined NAC-SAC from the WAC and hypothesised that during its closure, the present-day southern margin of the NAC was uplifted and eroded. These regions became the southern sources (Aileron Province and Tanami Region), which fed sediment into the greater McArthur Basin through a north-flowing drainage system. The ca. 1.4 to 1.35 Ga ocean closure/subduction related arc-volcanism (Kirkland et al., 2015) is temporally consistent with the juvenile neodymium isotopic compositions in the middle Velkerri Formation (Cox et al., 2016, 2019). Cox et al. (2016, 2019) suggested that the delivery of the arc volcanic detritus may have resulted in high nutrient supply to the basin, enhancing the primary productivity, and subsequent high organic carbon burial within the Velkerri Formation.

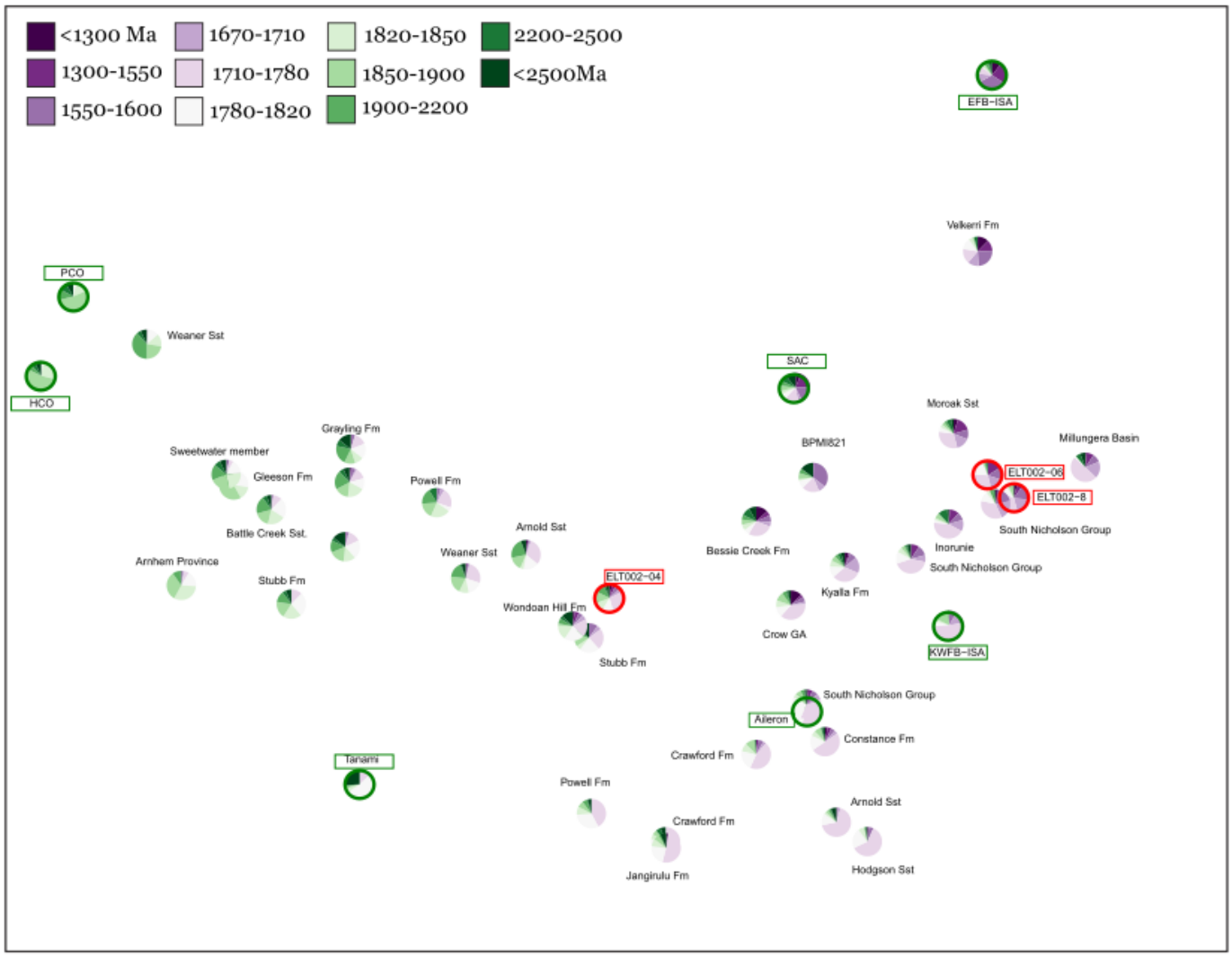

Figure 16: Multidimensional scaling (MDS) plot (after Vermeesch, 2013) showing relationship amongst analysed formations. Complied zircon age distribution from sedimentary units and potential sources plotted as pie diagrams, following the method proposed by Sharma et al. (2018). Detrita; 207Pb/206Pb age data included in the study are from Yang et al. (2018,2019), Munson et al. (2018), Carson (2013), Kositcin & Carson (2017), Nordsvan et al. (2018), Neumann & Kositcin (2011), Anderson et al. (2019) and Kositcin & Carson (2019), SAC: South Australian Craton; WFB: Western Fold Belt (Mount Isa Province); KFB: Kathleen Fold Belt (Mount Isa Province); EFB: Eastern Fold Belt (Mount Isa Province); Fm: Formation; Sst: Sandstone.

6. CONCLUSIONS

The ELT002 core was divided into three main broad sedimentological packages. First, at the bottom of the logged core is a tide-dominated delta, then the second package is interpreted as a river delta with significant fluvial influences. And the third package, top

of the core, is interpreted as a quiet pro-delta zone below wave base. Overall, each package represents a series of prograding deltaic parasequences, stacked to form a larger regressive system, where base level dropped, and the continent extended basinward. This is different to the type of depositional environment observed in Urapunga-4, where it is observed to be deposited in a low-energy off-shore marine environment (outer shelf to slope setting).

As for the geochemistry of the two cores, Urapunga-4 generally has more negative $\delta^{13}C_{(org)}$ values and higher TOC values compared to ELT002.

The trends in geochemistry observed in ELT002 show a positive correlation between $\delta^{13}C_{(org)}$ and TOC suggesting either increased bioproductivty to be the cause or it reflects a general trend of increasing maturity.

As for Urapunga-4, within the Amungee Member, the TOC peak seen in shale A is likely to be caused by increased primary production into an offshore environment OR sediment supply is out pacing the increased carbon production, causing sediment to swamp the organic matter. The B shale is interpreted to be a result of a small organic bloom that was immediately followed by increased sediment supply likely from a storm event. The C shale's TOC peak is also likely caused by primary production.

The new detrital U-Pb zircon ages and Rb-Sr dating constrained the ELT002 depositional window to be between 1412Ma to 1354Ma.

The Velkerri and Kyalla formations are sedimentologically and geochronologically most similar to those observed in ELT002. And using previous studies, found that the two standard deviation error windows for the lower succession of the ELT002 does just overlap with the permissive age of the Velkerri. However, more firmly overlaps with the age of the Kyalla Formation. This along with differences in geochemistry and

sedimentology between ELT002 and Urapunga-4, and the fact that ELT002 plots closer to the Kyalla on the MDS plot than the Velkerri, suggests that ELT002 represents, or at least intersects the Kyalla Formation.

7. ACKNOWLEDGMENTS

This honours project was funded by ARC Linkage LP200301457. I would like to thank my supervisors Alan Collins and Morgan Blades for their continued support throughout my honours. I would also like to thank Georgie Virgo, Darwin Subarkah, Tony Hall, the Martin Kennedy's Australian Shale Carbon Sequestration Group, and Adelaide Microscopy.

8. REFERENCES

Abbott ST, Sweet IP, Plumb KA, Young DN, Cutovinos A, Ferenczi PA, Brakel A and Pietsch BA, (2001). Roper Region: Urapunga and Roper River Special, Northern Territory (Second Edition). 1:250 000 geological map series explanatory notes, SD 53-10, 11. Northern Territory Geological Survey, Darwin and Australian Geological Survey Organisation, Canberra (National Geoscience Mapping Accord).

Abbott, S. T., & Sweet, I. P. (2000). Tectonic control on third-order sequences in a siliciclastic ramp-style basin: An example from the Roper Superbasin (Mesoproterozoic), northern Australia. Australian Journal of Earth Sciences, 47(3), 637-657. https://doi.org/10.1046/j.1440-0952.2000.00795.x

Ahmad M and Munson TJ (2013) Geology and Mineral Resources of the Northern Territory. Northern Territory Geological Survey 5

Ahmad, M., Dunster, J. N., & Munson, T. (2013). Ahmad M, Dunster JN and Munson TJ, 2013. Chapter 15: McArthur Basin: in Ahmad M and Munson TJ (compilers). 'Geology and mineral resources of the Northern Territory'. Northern Territory Geological Survey, Special Publication 5. 15, 11-72.

Anderson JR, Lewis CJ, Jarrett AJM, Carr L, Henson P, Carson C, Southby C and Munson T (2019) New SHRIMP U-Pb zircon ages from the South Nicholson Basin, Mout Isa Orogen, and Georgina Basin, Northern Territory and Queensland. Geoscience Australia, Record 10.

Baruch, E. T., Brenton, A. R., Close, D. I., Altmann, C. M., Mohinudeen, F. M., & Cote, A. J. (2018). The Kyalla Formation prospectivity from a mineralogical and sedimentological perspective [AGES Abstract]. https://geoscience.nt.gov.au/gemis/ntgsjspui/handle/1/87070

Bodorkos, S., Crowley, J. L., Claoué-Long, J. C., Anderson, J. R., & Magee Jr, C. W. (2021). Precise U–Pb baddeleyite dating of the Derim Derim Dolerite, McArthur Basin, Northern Territory: old and new SHRIMP and ID-TIMS constraints. Australian Journal of Earth Sciences, 68(1), 36-50. https://doi.org/10.1080/08120099.2020.1749929

Boyd, R., Dalrymple, R., & Zaitlin, B. A. (1992). Classification of clastic coastal depositional environments. *Sedimentary Geology*, *80*(3), 139-150. https://doi.org/https://doi.org/10.1016/0037-0738(92)90037-R

Canfield, D. (1994). Factors influencing organic carbon preservation in marine sediments. Chemical Geology, 114, 315-329. https://doi.org/10.1016/0009-2541(94)90061-2

Carson CJ (2013). The Victoria and Birrindudu Basins, Victoria River region, Northern Territory, Australia: a SHRIMP U-Pb detrital zircon and Sm-Nd study. Australian Journal of Earth Sciences 60, 175–96.

Chen, X., Zhou, Y., & Shields, G. A. (2022). Progress towards an improved Precambrian seawater

87Sr/86Sr curve. Earth-Science Reviews, 224, 103869. https://doi.org/https://doi.org/10.1016/j.earscirev.2021.103869

Claoué-Long, J., & Hoatson, D. (2005). Proterozoic mafic–ultramafic intrusions in the Arunta Region, central Australia: Part 2: Event chronology and regional correlations. Precambrian Research, 142, 134–158. https://doi.org/10.1016/j.precamres.2005.08.006

Claoué-Long, J., Maidment, D., Hussey, K., & Huston, D. (2008). The duration of the Strangways Event in central Australia: Evidence for prolonged deep crust processes. Precambrian Research, 166(1), 246-262. https://doi.org/https://doi.org/10.1016/j.precamres.2007.06.023

Close, D. F. (2014). The McArthur Basin: NTGS' approach to a frontier petroleum basin with known base metal prospectivity [AGES Abstract]. https://geoscience.nt.gov.au/gemis/ntgsjspui/handle/1/82357

Close, D. I., Mohinudeen, F. M., Altmann, C. M., Cote, A. J., Ilett, R., Richards, B., & Baruch, E. T. (2017). Proterozoic shale gas plays in the Beetaloo Basin and the Amungee NW-1H discovery [AGES Abstract]. https://geoscience.nt.gov.au/gemis/ntgsjspui/handle/1/85114

Collins, A. S., Higgie, D., Yang, B., Foden, J. D., Blades, M. L., Farkas, J., Dosseto, A., Subarkah, D., Nixon, A., Menpes, S., Edgoose, C., Warburton, J., Baruch-Jurado, E., Cassidy, E., Spagnuolo, S., Cox, G. M., Munson, T. J., Toledo, G., Glorie, S., Shannon, A. (2019). Life and times of the Proterozoic McArthur-Yanliao Gulf: Update on the ARC-Industry-NTGS Linkage Project [Presentation AGES Abstract]. https://geoscience.nt.gov.au/gemis/ntgsjspui/handle/1/88374

Collins, W. J., & Williams, I. S. (1995). SHRIMP ionprobe dating of short-lived Proterozoic tectonic cycles in the northern Arunta Inlier, central Australia. Precambrian Research, 71(1), 69-89. https://doi.org/https://doi.org/10.1016/0301-9268(94)00056-W

Cox, G. M., Collins, A. S., Jarrett, A. J. M., Blades, M. L., Shannon, A. V., Yang, B., Farkas, J., Hall, P. A., O'Hara, B., Close, D., & Baruch, E. T. (2022). A very unconventional hydrocarbon play: The Mesoproterozoic Velkerri Formation of northern Australia. AAPG Bulletin, 106(6), 1213-1237. https://doi.org/10.1306/12162120148

Cox, G. M., Jarrett, A., Edwards, D., Crockford, P. W., Halverson, G. P., Collins, A. S., Poirier, A., & Li, Z.-X. (2016). Basin redox and primary productivity within the Mesoproterozoic Roper Seaway. Chemical Geology, 440, 101-114. https://doi.org/https://doi.org/10.1016/j.chemgeo.2016.06.025

Crick, I. H. (1992). Petrological and maturation characteristics of organic matter from the Middle Proterozoic McArthur Basin, Australia. Australian Journal of Earth Sciences, 39(4), 501-519. https://doi.org/10.1080/08120099208728042

Crick, I. H. (1992). Petrological and maturation characteristics of organic matter from the Middle Proterozoic McArthur Basin, Australia. Australian Journal of Earth Sciences, 39(4), 501-519. https://doi.org/10.1080/08120099208728042

Crombez, V., Kunzmann, M., Faiz, M., Delle Piane, C., Munday, S., & Forbes, A. (2023). Stratigraphic architecture of the 1420–1210 Ma Velkerri and Kyalla Formations (Beetaloo Sub-basin, Australia). AAPG Bulletin, 107(11), 1901-1932. https://doi.org/10.1306/10152221163

Daly, A. R., & Edman, J. (1987). Loss of organic carbon from source rocks during thermal maturation (Vol. 71). https://doi.org/10.1306/42450Edman2019

Dirks, P. H. G. M., & Wilson, C. J. L. (1990). The geological evolution of the Reynolds Range, central Australia: evidence for three distinct structural-metamorphic cycles. Journal of Structural Geology, 12(5), 651-665. https://doi.org/https://doi.org/10.1016/0191-8141(90)90080-I

Frogtech Geoscience, 2018, SEEBASE® study and GIS for greater McArthur Basin. Northern Territory Geological Survey, Digital Information Package DIP 017. https://geoscience.nt.gov.au/gemis/ntgsjspui/handle/1/87064

George, S. C., & Ahmed, M. (2002). Use of aromatic compound distributions to evaluate organic maturity of the Proterozoic middle Velkerri Formation, McArthur Basin, Australia. In M. Keep, & S. J. Moss (Eds.), Proceedings of the Petroleum Exploration Society of Australia Symposium, The Sedimentary Basins of Western Australia 3 (pp. 253-270). Petroleum Exploration Society of Australia.

Hedges, J. I., & Keil, R. G. (1995). Sedimentary organic matter preservation: an assessment and speculative synthesis. Marine Chemistry, 49(2), 81-115. https://doi.org/https://doi.org/10.1016/0304-4203(95)00008-F

Hemingway, J. D., Rothman, D. H., Grant, K. E., Rosengard, S. Z., Eglinton, T. I., Derry, L. A., & Galy, V. V. (2019). Mineral protection regulates long-term global preservation of natural organic carbon. Nature, 570(7760), 228-231. https://doi.org/10.1038/s41586-019-1280-6

Howlett, D., Raimondo, T., & Hand, M. (2015). Evidence for 1808–1770 Ma bimodal magmatism,

sedimentation, high-temperature deformation and metamorphism in the Aileron Province, central Australia. Australian Journal of Earth Sciences, 62, 831-852. https://doi.org/10.1080/08120099.2015.1108364

Jackson MJ, Sweet IP and Powell TG, 1988. Studies on petroleum geology and geochemistry, Middle Proterozoic McArthur Basin, northern Australia I: Petroleum potential. APEA Journal 28, 283–302.

Jackson, S. E., Pearson, N. J., Griffin, W. L., & Belousova, E. A. (2004). The application of laser ablation-inductively coupled plasma-mass spectrometry to in situ U–Pb zircon geochronology. Chemical Geology, 211(1), 47-69. https://doi.org/https://doi.org/10.1016/j.chemgeo.2004.06.017

Johnston, D. T., Macdonald, F. A., Gill, B. C., Hoffman, P. F., & Schrag, D. P. (2012). Uncovering the Neoproterozoic carbon cycle. Nature, 483(7389), 320-323. https://doi.org/10.1038/nature10854

Kendall, B., Creaser, R. A., Gordon, G. W., & Anbar, A. D. (2009). Re–Os and Mo isotope systematics of black shales from the Middle Proterozoic Velkerri and Wollogorang Formations, McArthur Basin, northern Australia. Geochimica et Cosmochimica Acta, 73(9), 2534-2558. https://doi.org/https://doi.org/10.1016/j.gca.2009.02.013

Kennedy, M. J., Pevear, D. R., & Hill, R. J. (2002). Mineral surface control of organic carbon in black shale. Science, 295(5555), 657-660.

Kositcin N and Carson C (2017). New SHRIMP U-Pb zircon ages from the Birrindudu and Victoria basins,
Northern Territory: July 2016–June 2017. Geoscience Australia Record 2017/16.

Kositcin N and Carson CJ (2019) New SHRIMP U-Pb zircon ages from the South Nicholson and Carrara Range regions, Northern Territory: July 2017–June 2018. Geoscience Australia Record 2019/09.

Mukherjee, I., & Large, R. R. (2016). Pyrite trace element chemistry of the Velkerri Formation, Roper Group, McArthur Basin: Evidence for atmospheric oxygenation during the Boring Billion. Precambrian Research, 281, 13-26. https://doi.org/https://doi.org/10.1016/j.precamres.2016.05.003

Mukherjee, I., Large, R. R., Bull, S., Gregory, D. G., Stepanov, A. S., Ávila, J., Ireland, T. R., & Corkrey, R. (2019). Pyrite trace-element and sulfur isotope geochemistry of paleo-mesoproterozoic McArthur Basin: Proxy for oxidative weathering. 104(9), 1256-1272. https://doi.org/doi:10.2138/am-2019-6873 (American Mineralogist)

Munson, T. J. (2016). Sedimentary characterisation of the Wilton package, greater McArthur Basin, Northern Territory [NTGS Record](ISSN1443-1149 ISBN9780724573059 (PDF)). (NTGS Record 2016-003, Issue. https://geoscience.nt.gov.au/gemis/ntgsjspui/handle/1/83806

Munson, T. J., Whelan, J. A., Meffre, S., Zhukova, I., Woodhead, J. D., Thompson, J. M., & Beyer, E. E. (2018). Summary of results. NTGS laser ablation ICP-MS U-Pb and Lu-Hf geochronology project: Roper Group (McArthur Basin), overlying ungrouped units (Beetaloo Sub-basin), Renner Group (Tomkinson Province), and Tijunna Group (Birrindudu Basin) [NTGS Record](ISBN9780724573393 (PDF) ISSN1443-1149). (NTGS Record 2018-007, Issue. https://geoscience.nt.gov.au/gemis/ntgsjspui/handle/1/87656

Neumann NL and Kositcin N (2011) New SHRIMP U-Pb zircon ages from north Queensland, 2007–2010. Geoscience Australia, Record 2011/38, 1-82

Nixon, A. L., Glorie, S., Hasterok, D., Collins, A. S., Fernie, N., & Fraser, G. (2022). Low-temperature thermal history of the McArthur Basin: Influence of the Cambrian Kalkarindji Large Igneous Province on hydrocarbon maturation. Basin Research, 34(6), 1936-1959. https://doi.org/https://doi.org/10.1111/bre.12691

Nordsvan AR, Collins WJ, Li ZX, Spencer CJ, Pourteau A, Withnall IW, Betts PG and Volante S (2018) Laurentian crust in northeast Australia: implications for the assembly of the supercontinent Nuna. Geology 46, 251–54.

Norris A & Danyushevsky L (2018). 'Towards Estimating the Complete Uncertainty Budget of Quantified Results Measured by LA-ICP-MS', G., Boston, 2018-08-12.

Plumb KA and Roberts HG, 1992. The geology of Arnhem Land, Northern Territory. Mineral Provinces 15. Bureau of Mineral Resources, Record 1992/55.

Plumb, K. A., & WellmanPeter. (1987). McArthur Basin, Northern Territory; mapping of deep troughs using gravity and magnetic anomalies. BMR Journal of Australian Geology and Geophysics, 10(3), 243-251. https://eurekamag.com/research/019/384/019384853.php

Rafiei, M., & Kennedy, M. (2019). Weathering in a world without terrestrial life recorded in the Mesoproterozoic Velkerri Formation. Nature Communications, 10(1), 3448. https://doi.org/10.1038/s41467-019-11421-4

Rafiei, M., Löhr, S., Baldermann, A., Webster, R., & Kong, C. (2020). Quantitative petrographic differentiation of detrital vs diagenetic clay minerals in marine sedimentary sequences: Implications for the rise of biotic soils. Precambrian Research, 350, 105948. https://doi.org/https://doi.org/10.1016/j.precamres.2020.105948

Rawlings, D. J. (1999). Stratigraphic resolution of a multiphase intracratonic basin system: The McArthur Basin, northern Australia. Australian Journal of Earth Sciences, 46(5), 703-723. https://doi.org/10.1046/j.1440-0952.1999.00739.x

Rawlings, D., Korsch, R., Goleby, B., Gibson, G., Johnstone, D., & Barlow, M. (2004). The 2002 Southern McArthur Basin Seismic Reflection Survey. Geoscience Australia, 17.

Redaa, A., Farkaš, J., Hassan, A., Collins, A. S., Gilbert, S., & Löhr, S. C. (2022). Constraints from in-situ Rb-Sr dating on the timing of tectono-thermal events in the Umm Farwah shear zone and associated Cu-Au mineralisation in the Southern Arabian Shield, Saudi Arabia. Journal of Asian Earth Sciences, 224, 105037. https://doi.org/https://doi.org/10.1016/j.jseaes.2021.105037

Revie, D. (2017). Unconventional petroleum resources of the Roper Group, McArthur Basin [NTGS Record](ISBN9780724573134 (PDF) ISSN1443-1149). (NTGS Record 2017-002, Issue. https://geoscience.nt.gov.au/gemis/ntgsjspui/handle/1/85134

Rullkötter, J. (2003). Geochemistry, Organic. In R. A. Meyers (Ed.), Encyclopedia of Physical Science and Technology (Third Edition) (pp. 549-574). Academic Press. https://doi.org/https://doi.org/10.1016/B0-12-227410-5/00282-9

Scrimgeour, I. R., Kinny, P. D., Close, D. F., & Edgoose, C. J. (2005). High-T granulites and polymetamorphism in the southern Arunta Region, central Australia: Evidence for a 1.64Ga accretional event. Precambrian Research, 142(1), 1-27. https://doi.org/https://doi.org/10.1016/j.precamres.2005.08.005

Sharman, G., Sharman, J., & Sylvester, Z. (2018). detritalPy: A Python-based Toolset for Visualizing and Analyzing Detrital Geo-Thermochronologic Data. The Depositional Record, 4. https://doi.org/10.1002/dep2.45

Shen, Y., Knoll, A. H., & Walter, M. R. (2003). Evidence for low sulphate and anoxia in a mid-Proterozoic marine basin. Nature, 423(6940), 632-635. https://doi.org/10.1038/nature01651

Sheridan, M., Johns, D. R., Johnson, H. D., & Menpes, S. (2018). The stratigraphic architecture, distribution and hydrocarbon potential of the organic-rich Kyalla and Velkerri shales of the Upper Roper Group (McArthur Basin). The APPEA Journal, 58(2), 858-864. https://doi.org/https://doi.org/10.1071/AJ17224

Sláma, J., Košler, J., Condon, D. J., Crowley, J. L., Gerdes, A., Hanchar, J. M., Horstwood, M. S. A., Morris, G. A., Nasdala, L., Norberg, N., Schaltegger, U., Schoene, B., Tubrett, M. N., & Whitehouse, M. J. (2008). Plešovice zircon — A new natural reference material for U–Pb and Hf isotopic microanalysis. Chemical Geology, 249(1), 1-35. https://doi.org/https://doi.org/10.1016/j.chemgeo.2007.11.005

Subarkah, D., Blades, M. L., Collins, A. S., Farkaš, J., Gilbert, S., Löhr, S. C., Redaa, A., Cassidy, E., & Zack, T. (2022). Unraveling the histories of Proterozoic shales through in situ Rb-Sr dating and trace element laser ablation analysis. Geology, 50(1), 66-70. https://doi.org/10.1130/G49187.1

Subarkah, D., Nixon, A. L., Jimenez, M., Collins, A. S., Blades, M. L., Farkaš, J., Gilbert, S. E., Holford, S., & Jarrett, A. (2022). Constraining the geothermal parameters of in situ Rb–Sr dating on Proterozoic shales and their subsequent applications. Geochronology, 4(2), 577-600. https://doi.org/10.5194/gchron-4-577-2022

Summons, E., Boreham, Christopher, J., & TaylorDennis. (1994). Geochemical tools for evaluating petroleum generation in middle Proterozoic sediments of the McArthur Basin, Northern Territory, Australia. The APEA Journal, 34, Part 1, 692-706. https://eurekamag.com/research/019/003/019003296.php

Sweet IP and Jackson MJ, 1986. BMR stratigraphic drilling in the Roper Group, Northern Territory, 1985. Bureau of Mineral Resources, Australia, Record 1986/19

Tosca, N. J., Johnston, D. T., Mushegian, A., Rothman, D. H., Summons, R. E., & Knoll, A. H. (2010). Clay mineralogy, organic carbon burial, and redox evolution in Proterozoic oceans. Geochimica et Cosmochimica Acta, 74(5), 1579-1592. https://doi.org/https://doi.org/10.1016/j.gca.2009.12.001

Vermeesch, P (2013) Multi-sample comparison of detrital age distributions. Chemical Geology 341, 140-6

Walter, M. R., Veevers, J. J., Calver, C. R., & Grey, K. (1995). Neoproterozoic stratigraphy of the

Centralian Superbasin, Australia. Precambrian Research, 73(1), 173-195. https://doi.org/https://doi.org/10.1016/0301-9268(94)00077-5

Warren, J. K., George, S. C., Hamilton, P. J., & Tingate, P. (1998). Proterozoic Source Rocks: Sedimentology and Organic Characteristics of the Velkerri Formation, Northern Territory, Australia1. AAPG Bulletin, 82(3), 442-463. https://doi.org/10.1306/1D9BC435-172D-11D7-8645000102C1865D

Williams, B. (2019). Definition of the Beetaloo Sub-basin [NTGS Record](ISBN9780724573585 (PDF) ISSN1443-1149). (NTGS Record 2019-015, Issue. https://geoscience.nt.gov.au/gemis/ntgsjspui/handle/1/89822

Yang, B., Collins, A. S., Blades, M. L., Capogreco, N., Payne, J. L., Munson, T. J., Cox, G. M., & Glorie, S. (2019). Middle–late Mesoproterozoic tectonic geography of the North Australia Craton: U–Pb and Hf isotopes of detrital zircon grains in the Beetaloo Sub-basin, Northern Territory, Australia. Journal of the Geological Society, 176(4), 771-784. https://doi.org/10.1144/jgs2018-159

Yang, B., Collins, A., Blades, M., Munson, T., Payne, J., Glorie, S., & Farkas, J. (2020). Tectonic controls on sedimentary provenance and basin geography of the Mesoproterozoic Wilton package, McArthur Basin, northern Australia. Geological Magazine, 159, 1-20. https://doi.org/10.1017/S0016756820001223

Yang, B., Smith, T. M., Collins, A. S., Munson, T. J., Schoemaker, B., Nicholls, D., Cox, G., Farkas, J., & Glorie, S. (2018). Spatial and temporal variation in detrital zircon age provenance of the hydrocarbon-bearing upper Roper Group, Beetaloo Sub-basin, Northern Territory, Australia. Precambrian Research, 304, 140-155. https://doi.org/https://doi.org/10.1016/j.precamres.2017.10.025

Appendix A

Previously collected samples					collected from urapunga -4	
Depth (m)	**ID NUMBER**	**powder (Y/N)**	**Crushed (?)**	**Notes**	**ID number**	**Depth (m)**
37.30	213	y	-		u423A-01	18.2
40.20	212	n		sandstone	U423a-002	20
42.07	210	y	-		U423-02	29.9
44.50	209	y	-		U423a-03	22.5
48.95	208	n	y		U423a-04	24
50.65	207	n	y		U423a-05	26.4
53.80	206	y	-		U423a-06	28
59.45	219	y	-		U423a-07	46.9
62.05	204	y	-		U423a-08	77.35
64.84	218	y	-		U423a-09	80.8
68.60	203	n	y		U423a-10	92.6
72.55	202	y	-		U423-11	140.73
76.00	201	n	y	marker (?)	U423-12	144.8
78.90	199	n	y		U423-13	148.1
83.10	197	y	-		U423-14	155.6
88.55	196	y	-		U423-15	160
94.50	194	n	y		U423-17	173
97.15	191	n	y		U423-18	174.55
100.30	188	n	y		U423-19	175
103.35	183	n	y		U423-19 ? 20	209.45
107.20	181	n	y		U423-21	151.5
112.10	178	y	-		U423-22	159.25
116.15	177	n	y		U423-23	206.5
118.00	174	n	y		U423-24	302.7
120.30	170	n	y		U423-25	312
122.90	167	n	y	marker (?)	U423-27	226.98
125.20	166	n	y		U423-28	331.5
128.10	162	n	y		U423-29	345.7
130.30	160	n	y	marker (?)	U423-30	351.5
136.00	154	y	-		U423-31	369.5
138.70	151	n	y			
140.08	150	n	y			
144.40	147	y	-			
146.80	143	n	y			
149.04	140	n	y			
152.20	134	n	y			
155.50	130	y	-			
157.30	128	y	-			
161.35	126	n	y			
166.00	122	y	-			
168.90	120	n	y			
172.60	116	y	-			
175.50	113	n	y			
177.50	110	n	y			
180.50	109	y	-			
182.50	108	y	-			
187.20	106	y	-			
190.50	105	n	y			

193.00	104	y	-	
196.20	103	n	y	
199.20	101	y	-	
205.45	100	y	-	
206.70	98	n	y	
210.73	96	n	y	
212.80	95	n	y	
216.36	92	n	y	
219.00	82	y	-	
226.21	76	n	y	
229.00	77	n	y	
231.00	75	n	y	
237.38	74	n	y	
251.10	72	n	y	
253.87	71	n	y	
257.13	70	n	y	
261.59	69	n	y	
263.94	68	n	y	
267.60	67	y	-	
274.20	65	n	y	
278.20	64	n	y	
283.30	63	y	-	
286.64	62	y	-	
288.28	61	n	y	
293.91	60	y	-	
299.38	59	y	-	
304.52	58	n	y	
310.03	57	n	y	
315.03	55	y	-	
317.28	54	n	y	
320.73	53	y	-	
324.02	50	y	-	
326.00	47	y	-	
329.30	41	n	y	
335.52	38	n	y	
338.54	33	n	y	
341.44	29	n	y	
346.70	24	n	y	
349.00	16	n	y	
351.90	13	n	y	
355.45	10	n	y	
358.00	9	n	y	
360.55	8	y	-	
363.80	4	y	-	
371.20	2	y	-	
373.00	1	n		sandstone
174.60	114	y	y	

Appendix B

Urapunga-4 TOC			
Legacy data		New data	
TOC	depth	TOC	depth
0.00	18.80	1.67	18.2
0.00	26.40	0.61	20
0.00	32.30	1.77	22.5
0.18	37.30	0.81	24
0.00	39.70	1.1	26.4
0.09	41.70	1.38	28
0.41	42.07	0.19	46.9
0.19	44.50	0.69	77.35
0.00	46.90	0.32	80.8
0.27	53.80	0.69	92.6
0.28	59.45	11.7	140.73
0.38	62.05	5.04	144.8
0.84	64.84	7.84	148.1
0.32	72.55	1.68	151.5
0.62	74.40	1.96	151.5
0.55	77.35	5.41	155.6
0.48	80.80	1.86	159.25
0.42	83.10	8.31	160
0.39	88.55	5.18	173
0.95	92.60	5.54	174.55
1.32	95.65	2.07	175
0.11	95.95	1.8	206.5
1.16	98.00	2.91	226.98
0.58	99.70	1.57	302.7
0.47	102.30	1.71	312
	103.20	2.57	331.5
0.41	107.25	1.72	345.7
0.19	112.10	2.88	351.5
0.43	117.85	2.2	369.5
2.03	118.60		
4.39	127.60		
4.71	129.70		
5.59	132.55		
6.72	132.60		
6.61	132.60		
5.42	134.40		
5.31	134.40		
6.35	134.50		
11.49	136.00		
9.47	137.20		
6.18	137.60		
7.51	137.60		
9.88	140.78		
4.15	142.62		

ELT002 TOC	
TOC	Depth
0.9	217.5
0.89	221.8
0.83	224.5
0.83	228.8
0.84	232.5
0.82	235
0.82	240.7
0.86	244
0.87	248.2
0.82	252.4
0.79	256.8
0.8	259.6
0.48	264.5
0.46	268.5
0.44	271.2
0.7	276.9
0.42	283.6
0.44	287.7
0.44	291.5
0.44	296.6
0.43	300.9
1.01	514.4
0.88	517.8
1.06	522.6
1.06	526.9
1.09	531.3
1.04	535
0.89	539
0.99	544.7
0.87	548.3
0.94	552.5
1.04	556
0.83	559.7
0.74	564.7
0.78	567.4
0.98	572.9
2.65	576.8
0.6	580.7
0.55	583.7
0.9	592.1
0.88	596.6
0.65	600.4
0.83	604.8
0.98	607.7

7.33	144.40
2.69	144.75
2.64	144.80
3.41	145.60
4.61	148.10
5.06	148.33
2.71	152.20
5.03	155.50
5.28	155.60
0.67	155.70
7.46	157.25
6.79	157.30
8.68	157.30
6.23	158.60
5.27	160.00
5.87	163.70
7.12	166.00
4.15	168.10
3.21	170.05
3.76	172.60
3.15	173.00
1.31	174.55
2.96	174.60
3.54	175.00
3.49	175.50
2.93	180.50
2.14	182.50
2.04	187.20
1.01	193.00
3.63	196.20
4.49	199.20
1.90	205.45
4.81	206.50
1.88	206.53
2.72	209.37
3.82	209.50
3.38	210.73
5.28	212.20
3.88	216.90
3.70	217.59
2.17	218.75
	219.00
0.12	225.03
0.00	236.00
0.16	246.45
0.00	258.50
0.03	267.60

0.99	611.5
0.79	615.6
0.6	620.8
0.64	628.9
0.61	631.9
0.74	636.8
0.68	639.6
0.59	644.8
0.71	647.1
1.03	651.6
0.59	656.9
0.55	660.6
0.52	668.7
0.57	672.6
0.47	676.7

	283.30
	286.64
0.07	293.91
0.07	299.38
0.00	302.70
0.18	304.52
0.70	312.00
0.66	315.03
0.00	320.00
1.58	320.73
2.86	322.06
6.16	324.02
5.81	324.60
6.05	326.00
5.41	326.98
5.71	327.50
1.22	328.83
2.22	331.11
2.62	331.50
0.37	336.75
0.33	336.83
0.48	339.00
0.24	340.51
2.01	342.70
2.02	345.70
0.29	346.30
2.91	346.50
0.44	347.00
	347.47
1.71	348.20
3.31	348.20
0.52	348.83
1.64	351.10
2.14	353.20
2.39	354.72
2.23	357.00
2.27	358.00
2.13	360.30
4.06	363.44
0.54	363.80
0.47	369.50
1.11	369.73
0.20	371.20

Appendix C

U4 C Isotope+A1:HA1:H110

Sample	d13C	Precision
U4-134	-33.12	0.15
U4-140	-33.42	0.15
U4-143	-33.50	0.15
U4-143	-33.32	0.15
U4-147	-33.47	0.15
U4-150	-33.31	0.15
U4-151	-33.71	0.15
U4-151	-33.62	0.15
U4-160	-34.39	0.15
U4-160	-34.39	0.15
U4-162	-33.98	0.15
U4-167	-34.45	0.15
U4-170	-33.66	0.15
U4-174	-33.14	0.15
U4-177	No Beam	0.15
U4-178	No Beam	0.15
U4-181	-32.70	0.15
U4-183	-31.93	0.15
U4-183	-32.08	0.15
U4-188	-31.41	0.15
U4-194	-32.07	0.15
U4-194	-32.10	0.15
U4-196	-32.24	0.15
U4-197	-32.09	0.15
U4-199	-31.03	0.15
U4-201	-31.67	0.15
U4-202	-31.55	0.15
U4-203	-31.09	0.15
U4-204	-30.90	0.15
U4-204	-30.97	0.15
U4-206	No Beam	0.15
U4-207	-30.43	0.15
U4-208	-30.67	0.15
U4-209	No Beam	0.15
U4-210	-31.76	0.15
U4-213	No Beam	0.15
U4-218	-30.80	0.15
U4-219	-31.24	0.15
U423a-01	-33.06	0.15

ELT002 C Isotope

Name	Weight	d13C	Precision
ELT002-01	10.949	-30.11	0.18
ELT002-01	10.543	-22.26	0.18
ELT002-03	11.262	-26.07	0.18
ELT002-05	11.636	-28.28	0.18
ELT002-07	11.769	-28.66	0.18
ELT002-09	11.745	-28.50	0.18
ELT002-11	12.074	-28.93	0.18
ELT002-13	12.112	-28.19	0.18
ELT002-15	11.651	-28.70	0.18
ELT002-17	11.481	-28.07	0.18
ELT002-19	11.936	-28.32	0.18
ELT002-19	12.048	-29.02	0.18
ELT002-21	12.322	-23.90	0.18
ELT002-23	12.778	-28.54	0.18
ELT002-25	20.533	-28.35	0.18
ELT002-29	23.17	-28.44	0.18
ELT002-31	14.566	-33.70	0.18
ELT002-35	23.938	-30.23	0.18
ELT002-35	23.461	-28.97	0.18
ELT002-37	22.367	-29.66	0.18
ELT002-39	22.955	-28.76	0.18
ELT002-41	22.244	-28.34	0.18
ELT002-43	23.5	-28.43	0.18
ELT002-43	22.613	-27.48	0.18
ELT002-45	9.614	-31.82	0.18
ELT002-47	10.559	-31.77	0.18
ELT002-49	9.089	-31.90	0.18
ELT002-51	9.415	-31.85	0.18
ELT002-53	8.661	-32.04	0.18
ELT002-55	9.591	-31.87	0.18
ELT002-57	10.784	-31.86	0.18
ELT002-59	9.935	-31.66	0.18
ELT002-61	10.369	-32.20	0.18
ELT002-63	10.541	-32.07	0.18
ELT002-65	9.892	-31.41	0.18
ELT002-67	11.788	-31.75	0.18
ELT002-69	12.97	-31.56	0.18
ELT002-71	12.894	-31.97	0.18
ELT002-73	9.657	-32.77	0.18

U423a-01	No Beam	0.15
U423a-02	-32.39	0.15
U423a-03	-32.66	0.15
U423a-04	-32.45	0.15
U423a-05	-32.91	0.15
U423a-06	No Beam	0.15
U423a-07	No Beam	0.15
U423a-08	-32.05	0.15
U423a-08	No Beam	0.15
U423a-08	-32.04	0.15
U423a-09	-32.07	0.15
U423a-10	-32.85	0.15
U423a-10	-32.92	0.15
U423a-11	-33.40	0.15
U423a-11	-33.40	0.15
U423a-12	-33.22	0.15
U423a-13	-33.18	0.15
U423a-14	-33.20	0.15
U423a-15	-32.97	0.15
U423a-21	-32.44	0.15
U423a-22	-9.22	0.15
U4-100	-34.64	0.16
U4-101	-34.79	0.16
U4-101	-35.51	0.16
U4-103	-34.79	0.16
U4-104	-34.29	0.16
U4-105	-54.17	0.16
U4-105	-34.91	0.16
U4-106	-34.61	0.16
U4-108	-34.2	0.16
U4-113	-26.79	0.16
U4-116	-33.92	0.16
U4-120	-33.69	0.16
U4-122	-33.39	0.16
U4-126	-33.15	0.16
U4-126	-33.1	0.16
U4-13	-32.26	0.16
U4-16	-32.11	0.16
U4-2	-32.19	0.16
U4-24	-32.28	0.16
U4-29	-32.55	0.16
U4-38	-32.73	0.16
U4-4	-31.62	0.16

ELT002-75	3.814	-31.90	0.18
ELT002-75	3.573	-30.86	0.18
ELT002-77	16.121	-32.58	0.18
ELT002-79	17.374	-32.59	0.18
ELT002-79	17.657	-32.53	0.18
ELT002-83	10.515	-32.20	0.18
ELT002-85	10.351	-32.31	0.18
ELT002-87	14.446	-31.99	0.18
ELT002-89	11.471	-32.39	0.18
ELT002-89	11.7	-32.35	0.18
ELT002-91	9.5	-32.80	0.18
ELT002-93	9.594	-32.16	0.18
ELT002-93	8.767	-32.22	0.18
ELT002-95	11.95	-32.07	0.18
ELT002-97	15.539	-31.96	0.18
ELT002-101	14.999	-32.10	0.18
ELT002-101	16.038	-32.29	0.18
ELT002-103	15.552	-32.29	0.18
ELT002-105	12.425	-32.63	0.18
ELT002-107	13.746	-32.65	0.18
ELT002-107	15.062	-32.73	0.18
ELT002-109	16.216	-31.87	0.20
ELT002-111	13.641	-32.12	0.20
ELT002-113	9.563	-32.43	0.20
ELT002-115	16.528	-32.61	0.20
ELT002-117	17.346	-32.94	0.20
ELT002-121	18.297	-32.64	0.20
ELT002-123	17.02	No Beam	0.20
ELT002-125	18.076	-32.51	0.20
ELT002-127	26.683	-32.15	0.20
ELT002-129	16.481	No Beam	0.20
ELT002-129	16.394	-33.46	0.20
ELT002-131	26.215	-32.87	0.20
ELT002-133	16.878	-32.67	0.20
ELT002-133	16.994	-33.28	0.20
ELT002-135	17.035	-32.46	0.20
ELT002-137	13.886	-32.89	0.20
ELT002-139	13.508	-33.66	0.20
ELT002-139	13.176	-33.57	0.20
ELT002-141	14.354	-32.26	0.20
ELT002-143	30.671	-32.37	0.20
ELT002-145	13.798	-32.79	0.20
ELT002-147	20.548	-32.18	0.20

U4-41	-32.68	0.16
U4-47	-88.5	0.16
U4-53	-30.97	0.16
U4-53	-31.96	0.16
U4-54	-30.03	0.16
U4-55	-30.44	0.16
U4-58	-29.24	0.16
U4-74	-32.26	0.16
U4-8	-32.43	0.16
U4-82	-31.52	0.16
U4-9	-32.52	0.16
U4-9		0.16
U4-92	-35.42	0.16
U4-92	-30.62	0.16
U4-95	-35.03	0.16
U4-96	-34.85	0.16
U4-98	-34.62	0.16
U423a-17	-33.88	0.16
U423a-18	-34.06	0.16
U423a-19	-33.84	0.16
U423a-23	-34.25	0.16
U423a-24	-30.48	0.16
U423a-24	-30.89	0.16
U423a-25	-30.28	0.16
U423a-27	-30.63	0.16
U423a-27	-30.49	0.16
U423a-28	-32.5	0.16
U423a-29	-32.07	0.16
U423a-29	-32.45	0.16
U423a-30	-32.47	0.16
U423a-31	-32.96	0.16
U423a-31		0.16

ELT002-149	17.141	-32.32	0.20
ELT002-149	17.931	-32.09	0.20
ELT002-151	17.162	-32.57	0.20
ELT002-153	15.811	-32.43	0.20
ELT002-155	17.741	-32.28	0.20
ELT002-157	16.346	-32.24	0.20
ELT002-159	17.837	-32.96	0.20
ELT002-161	23.887	-32.33	0.20
ELT002-163	16.781	-32.47	0.20
ELT002-165	21.659	No Beam	0.20
ELT002-167	18.044	-32.5	0.20
ELT002-169	12.288	-32.63	0.20
ELT002-171	15.438	-32.25	0.20
ELT002-173	10.795	-32.59	0.20
ELT002-177	17.494	-32.42	0.20
ELT002-177	17.373	-32.79	0.20
ELT002-179	20.078	-32.85	0.20
ELT002-181	14.85	-33.99	0.20
ELT002-183	20.586	No Beam	0.20
ELT002-185	20.363	-33.63	0.20
ELT002-187	18.921	No Beam	0.20
ELT002-189	15.134	No Beam	0.20
ELT002-191	13.591	-32.98	0.20
ELT002-191	13.955	-33.44	0.20
ELT002-193	12.581	-33.23	0.20
ELT002-195	15.403	-32.83	0.20
ELT002-197	20.996	-32.84	0.20
ELT002-199	12.836	-33.21	0.20

Appendix D

LB#	Sample	Comment	CL image description	207Pb/206Pb Age (Ma)	207Pb/206Pb Age (Ma)	Concordia
482	ELT002-SST04 - 187		Weird Zoning (Possibly rim)	2506.2	49.2	94.0
367	ELT002-SST04 - 90	Ce spike in middle	same grain as 89 rim but closer to the core	2501.6	72.7	91.9
268	ELT002-SST04 - 09		no clear zoning	2424.2	30.6	96.9
486	ELT002-SST04 - 191		Core (not really any clear zoning)	1991.6	23.5	97.2
465	ELT002-SST04 - 176		Core?	1942.3	31.2	92.2
354	ELT002-SST04 - 83		same grain as 84	1922.1	31.0	97.1
484	ELT002-SST04 - 189		Zoning Core	1914.1	31.6	96.3
312	ELT002-SST04 - 47		weird zoning cannot see clearly	1891.6	31.9	93.8
458	ELT002-SST04 - 169	Al spike at start	No clear zoning	1886.0	32.9	94.4
315	ELT002-SST04 - 50		same grain as 49 rim but closer to the core compared to 49	1877.6	23.9	91.5
415	ELT002-SST04 - 132	Al spike at start	RIM same grain as 133	1862.1	33.3	95.3
431	ELT002-SST04 - 148		inner rim	1859.8	43.5	93.4
342	ELT002-SST04 - 71		weird zoning	1842.0	29.3	92.4
357	ELT002-SST04 - 86		weird zoning	1838.5	35.3	91.8
442	ELT002-SST04 - 153		Core	1820.9	32.8	93.7
353	ELT002-SST04 - 82		Core	1816.7	42.2	97.3
526	ELT002-SST04 - 231		Core	1810.6	39.7	91.4
452	ELT002-SST04 - 163		No clear zoning but spot is closer to the edge of the grain	1797.1	27.4	98.0
393	ELT002-SST04 - 116		Core same grain as 117	1779.8	27.8	94.0
261	ELT002-SST04 - 02		RIM very bright signal	1779.7	49.8	94.6
441	ELT002-SST04 - 152	Al spike at the start	dark no clear zoning	1768.5	32.1	90.7
277	ELT002-SST04 - 18		Rim	1767.5	36.6	91.3
521	ELT002-SST04 - 226		RIM same grain as 225	1759.1	28.3	92.7
425	ELT002-SST04 - 142		weird zoning cannot see clearly	1758.3	24.3	93.8
381	ELT002-SST04 - 104	Ugly	Rim but no clear zoning	1757.9	53.9	93.8
382	ELT002-SST04 - 105		no clear zoning.	1749.8	30.3	97.6
310	ELT002-SST04 - 45		Rim	1730.5	26.4	97.3
464	ELT002-SST04 - 175		Zoning Rim	1726.8	23.3	95.0
512	ELT002-SST04 - 217		Same grain as 216 CORE	1723.3	28.4	96.8
511	ELT002-SST04 - 216		Same grain as 217 RIM	1719.6	29.6	96.2
319	ELT002-SST04 - 54		No clear zoing same grain as 53	1714.6	26.9	95.3
302	ELT002-SST04 - 37		no clear zoing same grain as 36	1704.0	29.7	96.2

318	ELT002-SST04 - 53		No clear zoning but one of 2 spots (54 is on the same grain	1701.9	26.7	97.6
275	ELT002-SST04 - 16		no clear zoning	1701.6	33.8	91.9
333	ELT002-SST04 - 62		Weird zoning	1638.6	46.1	90.8
388	ELT002-SST04 - 111		Zoning core	1530.8	42.8	95.3
532	ELT002-SST04 - 237	spike at middle until er	core	**1396.1**	27.8	**92.9**

Appendix E

LB#	Sample	Comment	CL Image description	207Pb/206Pb Age (Ma)	207Pb/206Pb Age (Ma)	Concordance
155	ELT002-SST08 - 50		r	2499.5	42.2	97.7
59	ELT002-SST08 C - 47	Ew	Core	1883.5	40.2	91.1
226	ELT002-SST08 - 109		cannot see c	1873.8	55.8	95.4
158	ELT002-SST08 - 53		c same as 54	1873.3	35.2	94.5
98	ELT002-SST08 - 05		C	1872.9	34.1	91.1
208	ELT002-SST08 - 97		c	1862.6	28.2	93.1
197	ELT002-SST08 - 86		c	1850.9	22.1	96.0
190	ELT002-SST08 - 79		c	1825.6	38.5	92.7
213	ELT002-SST08 - 102		c? cannot see very well	1823.6	47.5	92.8
122	ELT002-SST08 - 23	Al spike at start	r same as 22	1819.9	33.8	95.6
43	ELT002-SST08 C - 31		C same as R13	1813.4	35.6	94.0
140	ELT002-SST08 - 41		c same as 42	1812.1	50.5	91.8
243	ELT002-SST08 - 126		r	1799.8	38.1	94.0
156	ELT002-SST08 - 51	Al spike near the end	rim?	1798.5	42.6	95.8
56	ELT002-SST08 C - 44		Core	1788.6	36.6	94.7
251	ELT002-SST08 - 134		cannot see clearly	1786.8	28.2	96.3
85	ELT002-SST08 R - 13		R same as C31	1782.3	33.2	95.0
214	ELT002-SST08 - 103		c? cannot see very well	1782.1	41.6	92.9
103	ELT002-SST08 - 10		messy but c same as 11	1779.2	47.3	93.3
53	ELT002-SST08 C - 41	Y spike early	C same as R18	1778.6	34.7	94.8
236	ELT002-SST08 - 119		c? not sure	1777.2	43.0	95.3
141	ELT002-SST08 - 42		r same as 41	1775.7	39.8	91.8
178	ELT002-SST08 - 73		r same as 72	1775.6	47.8	90.9
12	ELT002-SST08 C - 06		C same as R4	1775.6	31.6	91.5
137	ELT002-SST08 - 38	little Al spike near the end	outer rim same as 34	1774.1	42.6	92.7
70	ELT002-SST08 R - 04		R same as C6	1771.5	41.5	91.1
71	ELT002-SST08 R - 05		R same as C12	1771.3	30.6	94.6
108	ELT002-SST08 - 15		r	1770.5	34.0	94.0
144	ELT002-SST08 - 45		r	1769.2	33.1	98.2
229	ELT002-SST08 - 112		c	1769.0	36.7	95.3
28	ELT002-SST08 C - 22		Core	1768.9	32.7	95.6
223	ELT002-SST08 - 106		r? same as 87	1767.8	44.0	93.6
202	ELT002-SST08 - 91		c	1764.7	40.1	96.1

83	ELT002-SST08 R - 11		R same as C30	1762.6	34.6	91.2
121	ELT002-SST08 - 22	Al spike at start	c same as 23	1761.7	32.4	99.8
17	ELT002-SST08 C - 11		core	1759.9	32.9	97.5
188	ELT002-SST08 - 77		c	1759.1	41.8	94.6
230	ELT002-SST08 - 113		c not sure	1755.7	30.8	96.3
225	ELT002-SST08 - 108		cannot see	1755.0	32.9	98.4
237	ELT002-SST08 - 120		small zircon no clear zoning	1754.9	31.8	91.4
46	ELT002-SST08 C - 34		Core	1754.5	33.0	96.0
44	ELT002-SST08 C - 32		C same as R12	1744.0	28.3	94.6
117	ELT002-SST08 - 18		no clear zoning	1743.2	29.1	97.2
193	ELT002-SST08 - 82		r but messy	1742.2	39.8	97.4
99	ELT002-SST08 - 06		no clear zoning but C	1741.3	34.4	93.3
244	ELT002-SST08 - 127		small zircon no clear zoning	1740.7	30.5	97.3
18	ELT002-SST08 C - 12		C same as R5	1737.4	47.9	93.2
203	ELT002-SST08 - 92	Ugly	c	1736.2	26.9	96.7
207	ELT002-SST08 - 96		c? same as 104	1733.0	36.6	94.8
31	ELT002-SST08 C - 25		Core	1730.2	24.4	97.4
198	ELT002-SST08 - 87		c same as 106	1728.9	37.6	95.6
90	ELT002-SST08 R - 18		R same as C41	1727.6	35.1	97.8
49	ELT002-SST08 C - 37	Al going crazy	C same as R15	1724.1	37.2	94.7
240	ELT002-SST08 - 123		small no clear zoning	1723.6	34.4	94.8
87	ELT002-SST08 R - 15		R same as C37	1715.5	27.6	95.7
36	ELT002-SST08 C - 30		C same as R11	1712.1	43.9	95.8
143	ELT002-SST08 - 44		r same as 43	1705.5	43.6	95.7
136	ELT002-SST08 - 37	Al spike at the end	core? Same as 116	1702.1	36.5	93.0
125	ELT002-SST08 - 26		c but messy	1697.7	28.0	92.9
199	ELT002-SST08 - 88		core?	1697.6	42.3	98.1
138	ELT002-SST08 - 39	Al spike at start	possibly c same as 40	1696.5	39.4	93.9
23	ELT002-SST08 C - 17		C same as R7	1696.4	31.5	91.6
233	ELT002-SST08 - 116		r same as 37	1695.1	37.4	99.2
84	ELT002-SST08 R - 12	Al spike at start	R same as C32	1693.9	31.1	97.5
215	ELT002-SST08 - 104		c? same as 96	1693.9	27.7	90.5
161	ELT002-SST08 - 56	Al spike at start	c possibly same grain as 55	1690.4	24.3	95.6
20	ELT002-SST08 C - 14		Core	1690.4	28.2	95.6

127	ELT002-SST08 - 28	Al spikje at end	core but bright signal	1690.3	55.9	95.5
249	ELT002-SST08 - 132		cannot see clearly	1688.9	36.0	94.4
153	ELT002-SST08 - 48	signal al over the place	c?	1686.3	33.8	92.2
123	ELT002-SST08 - 24		noi clear zoning	1681.5	26.5	98.0
30	ELT002-SST08 C - 24		Core	1676.6	31.8	96.7
142	ELT002-SST08 - 43		c same as 44	1673.4	36.6	98.1
139	ELT002-SST08 - 40		rim? Same as 39	1673.3	28.4	98.6
133	ELT002-SST08 - 34	Al spike at end	inner rim same as 35	1671.2	31.4	97.3
134	ELT002-SST08 - 35	Al spike at end	outer rim same as 34	1670.3	29.0	98.0
107	ELT002-SST08 - 14		r same as 13	1667.0	31.6	94.8
173	ELT002-SST08 - 68		r same as 70	1665.0	28.6	96.4
92	ELT002-SST08 R - 20		R same as C53	1664.6	41.3	97.8
80	ELT002-SST08 R - 08		R same as C15	1658.3	37.8	93.9
224	ELT002-SST08 - 107		cannot see (not imaged)	1655.2	31.9	97.4
21	ELT002-SST08 C - 15		C same as R8	1653.1	28.7	94.5
204	ELT002-SST08 - 93		c	1645.5	28.3	93.9
9	ELT002-SST08 C - 03		C same as R3	1630.8	46.8	94.8
57	ELT002-SST08 C - 45		Core	1629.1	34.1	95.1
35	ELT002-SST08 C - 29		Core	1627.6	57.6	95.7
115	ELT002-SST08 - 16		c same as 17	1623.8	30.7	96.3
94	ELT002-SST08 - 01		C same as 02	1619.6	33.7	93.0
170	ELT002-SST08 - 65		c	1619.5	27.7	96.4
116	ELT002-SST08 - 17		r same as 16	1616.0	28.5	97.5
79	ELT002-SST08 R - 07		R same as C17	1609.2	40.6	100.2
55	ELT002-SST08 C - 43		Core	1605.7	34.7	90.5
152	ELT002-SST08 - 47	Al spike at start	c	1603.3	32.0	99.2
179	ELT002-SST08 - 74	ugly	c same as 75	1595.8	28.7	98.6
11	ELT002-SST08 C - 05	large Al spoike at the end	Core	1593.5	43.6	95.7
54	ELT002-SST08 C - 42		C same as R16	1582.4	61.2	96.9
247	ELT002-SST08 - 130		r same as c45	1580.6	33.8	96.5
14	ELT002-SST08 C - 08		Core	1577.9	31.5	95.3
86	ELT002-SST08 R - 14	Al spike in middle	**R same as C36**	1559.4	29.6	95.0
174	ELT002-SST08 - 69		not clear	1545.2	27.0	99.5
238	ELT002-SST08 - 121		skinny zircon no clear zononing	1513.8	33.9	92.9

88	ELT002-SST08 R - 16		R same as C42	1496.0	65.5	100.3
250	ELT002-SST08 - 133		cannot see clearly	**1379.6**	33.2	97.5

Appendix F

LB#	Source Filename	Comment	85Rb/86Sr->102	85Rb/86Sr->102
433	ELT002119 - 01.csv		7.0484	0.2096
434	ELT002119 - 02.csv		7.5996	0.5406
435	ELT002119 - 03.csv		8.1546	0.2810
436	ELT002119 - 04.csv		2.4245	0.2756
437	ELT002119 - 05.csv		6.6415	0.2310
438	ELT002119 - 06.csv		6.4533	0.1926
439	ELT002119 - 07.csv		6.2886	0.2828
440	ELT002119 - 08.csv		7.4227	0.4970
441	ELT002119 - 09.csv		7.6393	0.2780
442	ELT002119 - 10.csv		6.5154	0.2415
447	ELT002119 - 11.csv		7.0381	0.2262
448	ELT002119 - 12.csv		5.2064	0.2630
449	ELT002119 - 13.csv		1.5072	0.2840
450	ELT002119 - 14.csv		7.6413	0.2533
451	ELT002119 - 15.csv		14.5927	0.7734
452	ELT002119 - 16.csv		10.1487	0.4267
453	ELT002119 - 17.csv		7.2561	0.3014
454	ELT002119 - 18.csv		10.9707	0.6828
455	ELT002119 - 19.csv		7.2986	0.2604
456	ELT002119 - 20.csv		13.9524	0.5009
457	ELT002119 - 21.csv		5.2444	0.1935
458	ELT002119 - 22.csv		3.3010	0.2441
459	ELT002119 - 23.csv		7.8051	0.4074
460	ELT002119 - 24.csv		4.8522	0.3420
461	ELT002119 - 25.csv		8.5365	0.2747
462	ELT002119 - 26.csv		8.5276	0.6420
463	ELT002119 - 27.csv		5.3525	0.2963
464	ELT002119 - 28.csv		8.7526	0.3645
465	ELT002119 - 29.csv		11.1430	0.4243
466	ELT002119 - 30.csv		11.4012	0.4413
467	ELT002119 - 31.csv		6.6074	0.3464
468	ELT002119 - 32.csv		6.8840	0.3138
469	ELT002119 - 33.csv		8.0039	0.2709
470	ELT002119 - 34.csv		9.0959	0.3522
471	ELT002119 - 35.csv		6.1356	0.2452
472	ELT002119 - 36.csv		3.1651	0.2918
473	ELT002119 - 37.csv		8.2125	0.3057
474	ELT002119 - 38.csv		6.8585	0.3645
475	ELT002119 - 39.csv		12.6897	0.4402
476	ELT002119 - 40.csv		8.5721	0.2894
481	ELT002119 - 41.csv		7.2660	0.2672
482	ELT002119 - 42.csv		6.4724	0.3131
483	ELT002119 - 43.csv		5.7344	0.2387
484	ELT002119 - 44.csv		10.6889	0.3955
485	ELT002119 - 45.csv		5.7956	0.1998
486	ELT002119 - 46.csv		2.5634	0.3019

487	ELT002119 - 47.csv		7.1810	0.5070
488	ELT002119 - 48.csv		10.7292	0.3798
489	ELT002119 - 49.csv		0.6599	0.1522
490	ELT002119 - 50.csv		6.7692	0.3688
491	ELT002119 - 51.csv		9.2465	0.4144
492	ELT002119 - 52.csv		12.1028	0.4134
493	ELT002119 - 53.csv		6.4432	0.4851
494	ELT002119 - 54.csv		18.7909	1.3469
495	ELT002119 - 55.csv		7.5299	0.2694
496	ELT002119 - 56.csv		8.9308	0.4058
497	ELT002119 - 57.csv		7.8897	0.3224
498	ELT002119 - 58.csv		7.2495	0.3153
499	ELT002119 - 59.csv		3.9868	0.1529
500	ELT002119 - 60.csv		7.8109	0.3512
501	ELT002119 - 61.csv		9.6763	0.4037
502	ELT002119 - 62.csv		7.6665	0.5078
503	ELT002119 - 63.csv		8.0929	0.3291
504	ELT002119 - 64.csv		7.7788	0.2791
505	ELT002119 - 65.csv		5.2466	0.2790
506	ELT002119 - 66.csv		8.5288	0.3269
507	ELT002119 - 67.csv		7.9685	0.4428
508	ELT002119 - 68.csv		8.9623	0.3213
509	ELT002119 - 69.csv		7.7249	0.4852
510	ELT002119 - 70.csv		13.4200	0.4742
515	ELT002119 - 71.csv		8.4993	0.5124
516	ELT002119 - 72.csv		7.7542	0.3694
517	ELT002119 - 73.csv		5.6833	0.3515
518	ELT002119 - 74.csv		5.1121	0.3165
519	ELT002119 - 75.csv		8.7917	0.3271
520	ELT002119 - 76.csv		8.0108	0.4355
521	ELT002119 - 77.csv		6.3858	0.5996
522	ELT002119 - 78.csv		7.5083	0.2249
523	ELT002119 - 79.csv		9.8957	0.4175
524	ELT002119 - 80.csv		8.2545	0.3914

87Sr->103/86Sr->102	87Sr->103/86Sr->102	Rho: 207/206 vs 238/206
0.8492	0.0152	0.3569
0.8353	0.0195	0.8402
0.8570	0.0152	0.4113
0.7533	0.0156	0.6489
0.8310	0.0159	0.5410
0.8354	0.0160	0.7009
0.8097	0.0156	0.4060
0.8438	0.0179	0.7359
0.8465	0.0181	0.6939
0.8267	0.0153	0.5654
0.8378	0.0153	0.3186
0.8056	0.0160	0.5200
0.7460	0.0175	0.3236
0.8407	0.0165	0.4764
0.9825	0.0217	0.5950
0.8933	0.0181	0.4939
0.8384	0.0170	0.6227
0.9140	0.0201	0.5598
0.8373	0.0171	0.2752
0.9865	0.0193	0.5263
0.7981	0.0152	0.5842
0.7703	0.0144	0.6375
0.8450	0.0162	0.1588
0.8071	0.0167	0.5775
0.8544	0.0156	0.4064
0.8623	0.0198	0.4546
0.8180	0.0163	0.4423
0.8618	0.0179	0.4353
0.9090	0.0171	0.5895
0.9067	0.0178	0.5795
0.8176	0.0166	0.3738
0.8204	0.0172	0.5476
0.8465	0.0151	0.5549
0.8707	0.0169	0.5127
0.8206	0.0161	0.4354
0.7706	0.0150	0.5303
0.8487	0.0163	0.5367
0.8399	0.0166	0.6457
0.9050	0.0157	0.3007
0.8770	0.0152	-0.1019
0.8478	0.0164	0.4525
0.8356	0.0150	0.6151
0.8115	0.0154	0.5932
0.8778	0.0166	0.5615
0.8111	0.0159	0.4992
0.7479	0.0157	0.8303

0.8265	0.0194	0.7534
0.9085	0.0179	0.5909
0.7202	0.0189	0.4221
0.8463	0.0196	0.4967
0.8757	0.0176	0.5547
0.8938	0.0164	0.2042
0.8174	0.0172	0.6117
1.0888	0.0351	0.9365
0.8406	0.0157	0.5393
0.8408	0.0155	0.6132
0.8471	0.0161	0.5653
0.8393	0.0158	0.4459
0.7801	0.0137	0.2471
0.8534	0.0168	0.6073
0.8997	0.0176	0.4432
0.8561	0.0178	0.2791
0.8506	0.0153	0.5279
0.8529	0.0164	0.4143
0.8080	0.0152	0.4338
0.8840	0.0176	0.0662
0.8712	0.0175	0.5847
0.8780	0.0163	0.5229
0.8564	0.0175	0.6371
0.9750	0.0181	0.7845
0.8686	0.0193	0.7542
0.8590	0.0165	0.6167
0.8126	0.0165	0.7785
0.8100	0.0152	0.4989
0.8626	0.0166	0.4674
0.8732	0.0178	0.2009
0.8186	0.0204	0.6225
0.8380	0.0148	0.4845
0.8863	0.0176	0.7160
0.8437	0.0173	0.5742

Appendix G

LB#	Source Filename	Comment	85Rb/86Sr->102	85Rb/86Sr->102
637	ELT002807 - 01.csv		7.4935	0.3189
638	ELT002807 - 02.csv	Goes through inc, REE rich dont use te	25.0750	1.1754
639	ELT002807 - 03.csv	potential zr inclusions	9.7078	0.2992
640	ELT002807 - 04.csv	small zircon incl	7.1554	0.2308
641	ELT002807 - 05.csv	variable (not flat signal)	5.3159	0.2110
642	ELT002807 - 06.csv	variable (not flat signal)	5.9736	0.2796
643	ELT002807 - 07.csv	variable not flat 87sr	6.3484	0.2549
644	ELT002807 - 08.csv	variable not flat 87sr	6.1642	0.2507
645	ELT002807 - 09.csv		8.4607	0.3561
646	ELT002807 - 10.csv	zircon inclusions. Detrital	6.4287	0.2472
651	ELT002807 - 11.csv		11.6637	0.4035
652	ELT002807 - 12.csv		7.6620	0.2203
653	ELT002807 - 13.csv	variable zr	5.7732	0.2207
654	ELT002807 - 14.csv	incl... monazite potentially, REE variation	9.8813	0.3015
655	ELT002807 - 15.csv		9.6229	0.2956
656	ELT002807 - 16.csv		5.7298	0.1894
657	ELT002807 - 17.csv		6.4200	0.2997
658	ELT002807 - 18.csv	Quite variable TE esp zinc	8.3996	0.2647
659	ELT002807 - 19.csv	Variable TE esp cu and zn	11.9640	0.4351
660	ELT002807 - 20.csv		9.7388	0.3039
661	ELT002807 - 21.csv		6.2679	0.2306
662	ELT002807 - 22.csv	Variable TE incl with spike in REE	11.1486	0.4101
663	ELT002807 - 23.csv		6.9027	0.2211
664	ELT002807 - 24.csv	zrzr inc signal cut	6.6866	0.3985
665	ELT002807 - 25.csv	zr	10.0565	0.3819
666	ELT002807 - 26.csv	zr	8.0740	0.3858
667	ELT002807 - 27.csv		12.8137	0.4354
668	ELT002807 - 28.csv		6.9158	0.2305
669	ELT002807 - 29.csv		16.4883	0.6188
670	ELT002807 - 30.csv		7.6696	0.2486
671	ELT002807 - 31.csv		9.8197	0.3530
672	ELT002807 - 32.csv		7.6041	0.2520
673	ELT002807 - 33.csv		9.3108	0.4582
674	ELT002807 - 34.csv		7.6412	0.2354
675	ELT002807 - 35.csv	REE variable	9.9503	0.3575
676	ELT002807 - 36.csv		7.3538	0.2602
677	ELT002807 - 37.csv	Variable rb sr	3.7188	0.2002
678	ELT002807 - 38.csv		15.0064	0.7461
679	ELT002807 - 39.csv	variation in zr	16.1379	0.8004
680	ELT002807 - 40.csv		9.7377	0.3084
685	ELT002807 - 41.csv	inc in Fe	13.7199	0.4791
686	ELT002807 - 42.csv		8.4476	0.3448
687	ELT002807 - 43.csv	Zr	7.8750	0.2542
688	ELT002807 - 44.csv		5.8768	0.2426
689	ELT002807 - 45.csv		7.8255	0.2888
690	ELT002807 - 46.csv		6.4512	0.2453

691	ELT002807 - 47.csv	very variable	1.1794	0.0979
692	ELT002807 - 48.csv	zr inc	10.2020	0.3683
693	ELT002807 - 49.csv		6.4883	0.2418
694	ELT002807 - 50.csv	bad, inc Sr potentially ap inc	1.3829	0.1592
695	ELT002807 - 51.csv		12.3659	0.5668
696	ELT002807 - 52.csv		10.3986	0.3159
697	ELT002807 - 53.csv		8.1111	0.3203
698	ELT002807 - 54.csv		8.3354	0.3325
699	ELT002807 - 55.csv	short signal	3.0133	0.1178
700	ELT002807 - 56.csv	Titanium variable	8.1588	0.4205
701	ELT002807 - 57.csv		12.1271	0.3859
702	ELT002807 - 58.csv		8.4762	0.2835
703	ELT002807 - 59.csv		8.1568	0.2387
704	ELT002807 - 60.csv		11.6035	0.4205
705	ELT002807 - 61.csv		11.9246	0.5220
706	ELT002807 - 62.csv	some TE quite variable	14.5621	0.7981
707	ELT002807 - 63.csv		6.7908	0.2425
708	ELT002807 - 64.csv		9.6889	0.3195
709	ELT002807 - 65.csv	varibale signal	23.9736	1.3275
710	ELT002807 - 66.csv		12.5687	0.5139
711	ELT002807 - 67.csv		15.0689	0.4560
712	ELT002807 - 68.csv		9.8439	0.3324
713	ELT002807 - 69.csv	Zr icl	8.4461	0.2957
714	ELT002807 - 70.csv		3.9807	0.3200
719	ELT002807 - 71.csv		6.9567	0.2576
720	ELT002807 - 72.csv		14.3271	0.4880
721	ELT002807 - 73.csv		10.7320	0.3230
722	ELT002807 - 74.csv		13.9235	0.5331
723	ELT002807 - 75.csv		7.4197	0.2790
724	ELT002807 - 76.csv		7.6433	0.3041
725	ELT002807 - 77.csv	Zn Variable	10.9086	0.6974
726	ELT002807 - 78.csv		6.0250	0.2051
727	ELT002807 - 79.csv		12.9683	0.3921
728	ELT002807 - 80.csv		7.7223	0.3393

87Sr->103/86Sr->102	87Sr->103/86Sr->102	Rho: 207/206 vs 238/206
0.8417	0.0168	0.5187
1.2140	0.0289	0.4414
0.8825	0.0156	0.5882
0.8454	0.0154	0.5613
0.8075	0.0144	0.6173
0.8199	0.0153	0.6378
0.8234	0.0156	-0.0071
0.8228	0.0162	0.6342
0.8685	0.0176	0.5108
0.8257	0.0147	0.1240
0.9359	0.0186	0.5865
0.8334	0.0147	0.4094
0.8159	0.0149	0.5332
0.9122	0.0200	0.7696
0.9039	0.0188	0.3266
0.8243	0.0150	0.4898
0.8237	0.0174	0.6370
0.8712	0.0172	0.5829
0.9454	0.0201	0.5722
0.9062	0.0182	0.4048
0.8312	0.0146	0.6821
0.9319	0.0207	0.5150
0.8393	0.0156	0.2720
0.8388	0.0166	0.5043
0.9039	0.0159	0.7914
0.8749	0.0184	0.6578
0.9576	0.0182	0.3685
0.8364	0.0153	0.7911
1.0512	0.0253	0.6711
0.8660	0.0179	0.4566
0.9019	0.0192	0.6656
0.8552	0.0158	0.7118
0.8909	0.0228	0.3131
0.8583	0.0200	0.6709
0.9028	0.0206	0.4723
0.8570	0.0169	0.5052
0.7770	0.0180	0.8195
0.9977	0.0264	0.7517
1.0170	0.0224	0.5060
0.8814	0.0183	0.4191
0.9675	0.0197	0.6108
0.8680	0.0162	0.3909
0.8528	0.0160	0.4713
0.8121	0.0170	0.6639
0.8569	0.0174	0.6189
0.8406	0.0164	0.1304

0.7390	0.0165	0.5897
0.8836	0.0203	0.0876
0.8366	0.0142	0.9150
0.7273	0.0137	0.5660
0.9457	0.0197	0.6004
0.9133	0.0164	0.4641
0.8621	0.0173	0.3507
0.8685	0.0149	0.8174
0.7742	0.0206	0.5759
0.8543	0.0192	0.5451
0.9359	0.0179	0.4209
0.8748	0.0157	0.4750
0.8465	0.0150	0.7284
0.9226	0.0191	0.7097
0.9412	0.0216	0.6583
0.9848	0.0269	0.5795
0.8301	0.0156	0.3837
0.8914	0.0176	0.8721
1.1844	0.0338	0.7027
0.9481	0.0210	0.2219
0.9884	0.0190	0.2969
0.9119	0.0159	0.6270
0.8638	0.0147	0.6676
0.7994	0.0167	0.3529
0.8367	0.0172	0.6172
0.9862	0.0215	0.5582
0.9125	0.0169	0.6830
0.9699	0.0186	0.4241
0.8383	0.0156	0.4252
0.8518	0.0153	0.4340
0.9455	0.0270	0.2831
0.8335	0.0141	0.6041
0.9722	0.0181	0.4452
0.8550	0.0166	0.4510